Source attribution of European surface O_3 using a tagged O_3 mechanism

Aurelia Lupaşcu[1] and Tim Butler[1,2]

[1]Institute for Advanced Sustainability Studies (IASS), Potsdam, 14467, Germany
[2]Freie Universität Berlin, Institut für Meteorologie, Berlin, Germany

Correspondence: A.Lupascu (Aurelia.Lupascu@iass-potsdam.de)

Abstract.

Tropospheric ozone (O_3) is an important air pollutant that affects human health, ecosystems, and climate. The contributions of O_3 precursor emissions from different geographical source regions to the O_3 concentration can help to quantify the effects of local versus remote transported precursors on the O_3 concentration in a certain area. This study presents a "tagging" approach within the WRF-Chem model that attributes O_3 concentration in several European receptor regions to nitrogen oxides (NO_x) emissions from within and outside of Europe during April-September 2010. We also examine the contribution of these different precursor sources to various O_3 metrics and their exceedance events. Firstly, we show that the spatial distributions of simulated monthly mean MDA8 from tagged O_3 sources regions and types for late spring, summer and early autumn 2010 varies with season. For summer conditions, O_3 production is dominated by national and intra-European sources, while in the late spring and early autumn intercontinental transported O_3 is an important contributor to the total O_3 concentration. We have also identified shipping activities in the Mediterranean Sea as an important source of O_3 for the Mediterranean countries, as well as the main contributor to high modelled MDA8 O_3 concentration in the Mediterranean Basin itself. Secondly, to have a better understanding of the origin of MDA8 O_3 exceedances, we compare modelled and observed values of MDA8 O_3 concentration in the "Po Valley" and "Germany-Benelux" receptor regions, revealing that the contribution from local sources is about 41 % and 38 % of modelled MDA8 O_3 during the exceedances days respectively. By examining the relative contributions of remote NO_x sources to modelled and observed O_3 exceedance events, we determine that model underrepresentation of long-range O_3 transport could be contributing to a general underestimation of modelled O_3 exceedance events in the Germany-Benelux receptor region. Thirdly, we quantify the impact of local vs. non-local NO_x precursors on O_3 production for each European receptor region using different O_3 metrics. The comparison between mean, MDA8 and 95th percentile O_3 metrics accentuate the importance of large contributions from locally-emitted NO_x precursors to the high-end of the O_3 distribution. When we compare the vegetation and health metrics, we notice that the SOMO35 and AOT40 indexes exhibit rather similar behaviour, while the W126 index accentuates the importance of local emissions. Overall, this study highlights the importance of a tagging approach to quantify the contribution of local and remote sources to the MDA8 O_3 concentration during several periods as well to different O_3 metrics. Moreover, this method could be applied to assess different mitigation options.

1 Introduction

Tropospheric ozone (O_3) is formed primarily during the oxidation of volatile organic compounds (VOC) in the presence of nitrogen oxides (NO_x) and sunlight. Ground-level O_3 is an important air pollutant that damages human health (Fleming et al., 2018) and vegetation (Mills et al., 2018). It also affects the radiative forcing (e.g. Ramaswamy et al., 2001; Stevenson et al., 2013), and therefore contributes to climate change. Impacts of O_3 on human health are associated with lung disease, chronic disease and death from respiratory ailments. To protect human populations from exposure to high levels of O_3, the World Health Organization (WHO, 2006, 2017) recommended an air quality guideline for ozone in which the maximum daily average 8-h (MDA8) for O_3 should not exceed 100 $\mu g\ m^{-3}$. The European Environmental Agency (EEA, 2017a) reported that the EU long-term objective target concentration of 120 $\mu g\ m^{-3}$ is often exceeded and that more than 90 % of the urban population of the European Union was exposed to O_3 levels higher than the stricter recommendation set by the WHO. A 2010 report from HTAP (HTAP, 2010) shows that the observed baseline O_3 concentrations (concentrations without the contribution from local anthropogenic emissions) have increased throughout the last several decades since overall global anthropogenic emissions of O_3 precursors have increased. However, a more recent study by Gaudel et al. (2018) has established that the global surface O_3 trends exhibit high variability, and depend on several factors such as season, region, elevation and proximity to fresh ozone precursor emissions. However, since the network capable of monitoring ozone levels is sparse, it is difficult to quantify the O_3 changes on a global scale. Satellite-derived O_3 measurements can be used to quantify changing levels of O_3, but Gaudel et al. (2018) showed that these products are not capable of quantifying significant trends. Surface O_3 pollution due to urbanization and motorization processes are serious challenges for large cities (e.g. Chan and Yao, 2008; Folberth et al., 2015; Li et al., 2017, 2019). Paoletti et al. (2014) showed that in Europe and the United States of America, the average O_3 concentration in the cities has increased at a faster rate than those observed in rural areas. Fleming et al. (2018) showed that the 4th highest daily maximum 8-hour O_3 (4MDA8) is more ubiquitous at urban sites than at non-urban sites. This leads to a worsening of general air quality that, ultimately, affects human health and ecosystems (Paoletti et al., 2014; Monks et al., 2015; WHO, 2017; Fleming et al., 2018; Mills et al., 2018). To improve the air quality in certain areas, it is important to know the extent to which different precursors (NO_x and VOCs) contribute to tropospheric O_3 concentrations.

Information regarding levels of NO_x and VOC emissions and weather conditions enhances our ability to predict the formation of tropospheric O_3. The continuous development of chemical transport models can lead to a better understanding of the processes that contribute to high-O_3 episodes. Knowing the impacts of NO_x and VOC emissions from sources such as surface anthropogenic activities, fires, soil, and the stratosphere on total O_3 production can help authorities develop strategies aimed at reducing the impact of high levels of O_3 on the well-being of both humans and ecosystems. Several approaches have been used to determine the extent to which individual sources contribute to total levels of O_3. For example, perturbation of different emission categories have allowed scientists to make estimations regarding the contributions of individual sources of O_3 to total O_3 levels (e.g. Fiore et al., 2009).

Tagging techniques have also been used in modelling studies to determine source/receptor relationships and how individual sources of pollutants contribute to total pollution levels at given locations. Pollutants with relatively low chemical reactivities,

such as carbon monoxide (CO), can be "tagged" according to their emission sectors or regions for attribution studies (e.g. Pfister et al., 2011). Sudo and Akimoto (2007), and Derwent et al. (2015) used O_3 tracers tagged by their region of formation to show that intercontinental transport of O_3 can occurring from polluted source regions, such as North America and East-Asia, appears to be the most important source of tropospheric O_3 in Europe. Other studies, including those of Wang et al. (2009) and Grewe

5   et al. (2010, 2012, 2017) have used tagging methods to identify the contribution of individual sources of O_3 to overall levels. This method is especially useful since it can track emitted NO_x species during transport and chemical processing. Moreover, Grewe et al. (2012) showed the impact of the tagging method on mitigation measures, while Dahlmann et al. (2011) examined the contribution of O_3 sources to O_3 radiative forcing. Work by Emmons et al. (2012) and Butler et al. (2018) describe a procedure for tagging O_3 produced from NO_x sources through updates to the MOZART chemical mechanism, and Butler et al.

10   (2018) expanded the tagging technique to account for VOC sources.

Based on the work of Emmons et al. (2012), Pfister et al. (2013) and Safieddine et al. (2014) were able to use the WRF-Chem regional model to quantify the contribution of inflow (tagged O_3 and odd nitrogen species entering into the regional domain at the lateral boundaries) and of anthropogenic NO_x precursors (named NO_x in the following) on the surface O_3 levels. Using a slightly different methodology, Gao et al. (2016) have implemented within WRF-Chem framework a tagging method based

15   on Ozone Source Apportionment Technology (OSAT) (Yarwood et al., 1996) incorporated in the Comprehensive Air quality Model with extensions (CAMx).

Much effort has been focused understanding the origin of tropospheric O_3 and the key role played by the intercontinental transport, the contribution of stratospheric O_3 intrusion, and of different emissions sources to tropospheric O_3 concentration in a wide range of receptor regions. To better understand the changes in air pollution levels, it is necessary to know the relationship

20   between levels of an emitted species and its atmospheric concentration. When this information is available, it is possible to quantify the contribution of different emission precursor sources to overall O_3 concentration levels at a particular receptor location. For this purpose, we followed a strategy outlined in Emmons et al. (2012) and Butler et al. (2018) to implement a tagging technique into the regional WRF-Chem model. The model can be used to quantify source contributions to the tropospheric O_3 concentration, by "tagging" NO_x emissions, and corresponding products so that they can be traced to the final

25   production of O_3.

When studying the effects of O_3, the impact of the compound on humans and vegetation is of the utmost importance. Therefore, several exposure indexes have been defined to describe the relationship between O_3 and both human health and agricultural crop yield that are based on hourly averaged data. Musselman et al. (2006), Agathokleous et al. (2018), and Lefohn et al. (2018) review literature describing O_3 metrics. Additionally, a work by Paoletti et al. (2007) has provided a list of

30   common O_3 exposure metrics used to assess risk to human health and vegetation. Here we use some well-known O_3 metrics, such as MDA8, SOMO35, AOT40, and W126. The MDA8 index has been defined as the maximum daily average 8-h (MDA8) O_3 values (ppb) (Lefohn et al., 2018). SOMO35 (WHO, 2001) has been determined by European protocols (EU directive 2008/50/EC, 2008) and is defined as the annual sum of MDA8 O_3 with a cut-off of values of 35 ppb. Both MDA8 and SOMO34 are health-related metrics. The AOT40 and W126 vegetation metrics have been used to regulate air pollution in both Europe

35   (EU directive 2008/50/EC, 2008) and the United States (U.S. EPA regulations https://www.gpo.gov/fdsys/pkg/FR-2015-10-

26/pdf/2015-26594.pdf). European legislation (EU directive 2008/50/EC, 2008) AOT40 metric is measured throughout daytime periods from May to July (growth season) and has a defined target limit of 18000 μg m^{-3} h (9000 ppb $-$ hours) and a long term objective of 6000 μg m^{-3} h (3000 ppb $-$ hours). A standard of 15 ppm $-$ hours has been defined for the seasonal W126 index, which is averaged over three years. These metrics have been used to assess the impact of mitigation strategies (Avnery

5 et al., 2013), the impact of industry on air quality management issues (Vijayaraghavan et al., 2016), and the impact of high O$_3$ levels and temperatures on crops (Tai and Val Martin, 2017).

In this paper, we use a tagged O$_3$ mechanism in the WRF-Chem model to understand the contribution of emitted O$_3$ precursors from different geographical source regions and types on the modelled O$_3$ concentration in several European receptor regions. In Section 2 we discuss the details of implementing this tagging technique, and describe changes made to both the

10 chemical mechanism and WRF-Chem code. Section 2 also describes the WRF-Chem configuration, simulation design, and input data used in the study. An analysis of the WRF-Chem simulation is presented in Section 3, while Section 4 summarizes our findings.

2 Model simulation

2.1 Tagging technique

15 To perform a WRF-Chem model simulation using a tagging approach, several changes must be implemented in the model code to accommodate additional tracers and reactions representing tagged constituents. Butler et al. (2018) describes in detail how the tagging technique was implemented in the Community Earth System Model. The tagging technique used in this study is based on the same approach and uses the same modified version of the MOZART chemical mechanism. Further detail on how the chemical mechanism was extended can be found in Butler et al. (2018).

20 To use the NO$_x$ tagging mechanism, a new chemistry option was added in the namelist.input file: chem_opt=113 and through the code. The coupling of the new chemical scheme with microphysics and radiative processes requires several modifications to the code: 1) The first step is to create a new chemistry option. The package mozart_tag_kpp (chemopt==113) has been added to ~/WRFV3/Registry/registry.chem together with new model variables for tagged NO$_x$ species (e.g. O3_X_INI, O3_X_STR, etc). For this purpose, the pre-processing software described in Butler et al. (2018) was adapted to produce

25 a new chemical mechanism; 2) The new chemistry package is a KPP option. Therefore, we created a new subdirectory in ~/WRFV3/chem/KPP/mechanisms/ directory containing the files (*.spc, *.eqn, *.kpp, and *.def) which defined the chemical model species and constants, chemical reactions in KPP format, model description, computer language, precision, and integrator.

The new chemistry option considers a large number of species and reactions; therefore we exceeded hard-coded limits

30 that the KPP chemical preprocessor, version 2.1 (Sandu and Sander, 2006) allows. To overcome these limits, we increased MAX_EQN and MAX_SPECIES in the header file gdata.h, located in ~/WRFV3/chem/KPP/kpp/kpp-2.1/src. Further, we updated the subroutines in the ~/WRFV3/chem directory to consider the new chemistry package. The modules that we modified are described in the Appendix.

Although WRF-Chem uses the Advanced Research WRF (ARW) dynamic core in this simulation which conserves mass and scalar mass (Grell et al., 2005), the tagged O_3 species are advected independently. Thus, numerical errors associated with the advection scheme led to gradients in the sum of tagged species concentration compared to the "real" concentration; therefore, the relationship between these variables is not conserved. Since the advection scheme fails to reproduce the expected solution (in which the sum of the tagged species concentration at each grid point must be equal to "real" concentration), we solve this by fixing all undershoots and/or overshoots assuming that the sum of tagged species mass is proportional to the "real" concentration. This technique was also applied in Flemming et al. (2015), and Gromov et al. (2010).

Compared to Pfister et al. (2013) and Safieddine et al. (2014) work, the expanded tagging technique used in this study has the advantage that multiple tags can be defined in each model run.

2.2 Experimental setup

WRF-Chem version 3.7.1 was used for this study to account for the impact of different global and European O_3 precursor source regions to several European receptor regions during the April-September 2010 period. A single domain, that covers the area between 32° N and 70° N, and 29° W and 57° E, was used with 50-km grid spacing and 35 vertically-stretched layers from the ground up to 50 hPa. The physics options used for this study include the Morrison double-moment microphysics scheme (Morrison et al., 2009), the Grell-Freitas cumulus parameterization (Grell and Freitas, 2014), the Rapid Radiative Transfer Model (Iacono et al., 2008) for longwave and Goddard shortwave scheme (Chou and Suarez, 1994), the Yonsei University boundary-layer parameterization (Hong et al., 2006), and the Monin-Obukhov scheme for the surface layer (Jiménez et al., 2012). The initial and boundary conditions for meteorological fields are taken from the European Centre for Medium-Range Weather Forecasts (ECMWF) reanalysis. Anthropogenic emissions were obtained from the TNO-MACC III emission inventory for Europe (Kuenen et al., 2014). Because the model domain extends beyond the edges of the TNO-MACC III inventory, we used for completion emissions from the HTAP V2 inventory (http://edgar.jrc.ec.europa.eu/htap_v2). Biogenic emissions were computed on-line using the Model of Emissions of Gases and Aerosols from Nature (MEGAN) model (Guenther et al., 2006). The biomass burning emissions are based on Fire INventory from NCAR (FINN) (Wiedinmyer et al., 2011).

For this WRF-Chem simulation, the tagged MOZART chemical mechanism for NO_x emissions (Butler et al., 2018) is used to represent the gas-phase chemistry. The photolysis rates were computed using the Fast Tropospheric Ultraviolet and Visible (FTUV) Radiation Model (Tie et al., 2003; Li et al., 2005). The dry deposition was calculated following the Wesely (1989) resistance method, while the wet removal scheme for the tagged MOZART chemistry is based on Neu and Prather (2012).

NOx emitted by several source regions and types are tagged and explicitly tracked using additional tagged reactions and tracers. Thus, we follow the contribution to the total ozone concentration from each specific emission source and type, from both within and outside the European model domain. Table 1 summarizes tagged sourceis regions and types that are used in this study. Using a division of source regions within the European model domain, 15 geographical source regions are specified in Table 1 and depicted in Figure 1. A similar division of European regions has been used by Christensen and Christensen (2007) and Otero et al. (2018) to address the main sources of uncertainty in regional climate simulations, as well as during the AQMEII project (i.e. Struzewska et al., 2015). Except for ALP, the source regions within the European domain are identical to

receptor regions. Given the complex topography of the ALP source region, we split this region into two receptor regions: the Po Valley region and the high Alps (regions above 1500 m elevation).

To represent the impact of transported O_3 from different regions outside of the domain, we used chemical boundary conditions derived from the extended CAM-Chem version 1.2 global simulations. Butler et. al (in preparation) used the tagging approach within the CAM-Chem model for several HTAP2 source regions such as: ASI (Asia), NAF (North-Africa), NAM (North-America), OCN (Oceanic sources), RBU (Russia, Belarus, Ukraine), and RST (rest of the world), as well as for several other source types: BIO (biogenic emissions), BMB (biomass burning emissions), LGT (lightning), and STR (stratospheric O_3). No overlap of source regions or types is allowed.

The BIO, BMB, LGT, and STR source types are also included in the tagged chemical mechanism used in this simulation, but without including them into the division of source regions; we refer to these sources as "other global source types" from here on. Ozone due to these other global source types can originate both from long-range transport from remote source regions through the lateral model boundaries as well as from precursor emissions within the European model domain.

For each receptor region, we analyse the impact of the NO_x emissions coming from different source regions and types to the total O_3 concentration.

2.3 Ozone metrics

Using different metrics to assess the impact of O_3, we can determine which precursor sources most highly influence the accumulation of O_3 in different receptor regions, and thus to provide insights into which type of mitigation measures will be useful for a particular geographic area. These metrics include the mean O_3 concentration, the mean of MDA8, the cumulative exposure to mixing ratios above 35 ppb (SOMO35) (Colette et al., 2012), and the 95th percentile for surface O_3. Neither the impact of O_3 exposure on trees, plants and ecosystems (W126) (Lapina et al., 2014), nor the AOT40 accumulation metric (the threshold is 40 ppb) were used to assess risk to vegetation from O_3 exposure (UNECE, 2010).

The European Air Quality Directive (EU directive 2008/50/EC, 2008) specifies that O_3 exposure should remain below a target MDA8 O_3 value of 120 μg m^{-3}, which can be exceeded up to 25 days per calendar year averaged over three years. The modelled daytime AOT40 (during local daylight hours 8 AM – 7 PM) was calculated according to Equation (1).

$$AOT40 = \sum_{i=1}^{90 \text{ days}} \left(\sum_{h=8}^{19} max\left(O_{3i,h} - 40, 0\right) \right) \qquad (1)$$

According to European legislation (EU directive 2008/50/EC, 2008), the AOT40 metric is accumulated over the daytime period from May to July (growth season) and it has a defined target limit of 18000 μg m^{-3} h (9000 ppb $-$ hours) and a long term objective of 6000 μg m^{-3} h (3000 ppb $-$ hours). W126, however, is described according to U.S. EPA regulations (https://www.gpo.gov/fdsys/pkg/FR-2015-10-26/pdf/2015-26594.pdf). A standard of 15 ppm $-$ hours is defined for the seasonal W126 index, which is an average over a three-year period. For this study, the hourly surface O_3 tagged outputs for April

through September are used to calculate the highest 3-month W126 index values (see Eq. 2):

$$W126 = \sum_{i=1}^{90 \text{ days}} \left(\sum_{h=8}^{19} O_{3i,h} \cdot \left(\frac{1}{1 + (4403 \cdot e^{-126 \cdot O_{3i,h}})} \right) \right) \tag{2}$$

According to Lefohn et al. (1988), the W126 index includes all hourly O_3 values within the specified time range, although a lower weight is given to hourly O_3 concentrations below the inflection point of 65 ppb, while values above 90 ppb are weighted with a factor of almost one. SOMO35 (WHO, 2001) is defined as the sum of the MDA8 O_3 with a cut-off of 35 ppb (see Eq. 3). For this metric, the EU air quality directives do not prescribe a limit or a target values.

$$SOMO35 = \sum_{h=1}^{6 \text{ months}} max\left(MDA8_i - 35, 0.0\right) \tag{3}$$

The contribution of tagged O_3 is based on formulations of each metric and is calculated from the model output. In the case of the MDA8 and 95th percentile metrics, we searched for the specific period in which calculated values of total O_3 concentration meet the requirements for the formulation of these metrics. Once this is identified, tagged O_3 concentrations are extracted for the same period which can then be used for further analysis. However, the contribution of concentration of tagged O_3 on cumulative metrics is slightly different, a large proportion of each tagged species is used to determine total O_3, as illustrated below for AOT40 at a specific time period:

$$AOT40_{tag} = \sum_{i=1}^{90 \text{ days}} max\left((O_3 - 40.) \cdot \frac{O_{3,tag}}{O_3}, 0.0 \right) \tag{4}$$

Based on their formulation, we grouped metrics into either non-cumulative (mean O_3, MDA8, and the 95th percentile) or cumulative (SOMO35, W126, and AOT40) categories. Since the latter metrics have different formulations (including hourly O_3 values above a specific threshold) and do not cover the same periods, to facilitate a more direct comparison between findings from multiple O_3 metrics, an analysis of the relative contribution of different source regions to total O_3 in each receptor region was performed. This was done using averaged values for non-cumulative metrics, and 6-month sums for SOMO35, AOT40, for cumulative metrics useful for evaluating effects on crops (cumulated over May-July period) and a maximum of 3-month sums for every consecutive 3-month period determined using the W126 index.

3 Results and discussions

Our discussion of the results of the model is focused on the April-September 2010 period. We first briefly evaluate the ability of WRF-Chem to reproduce meteorological parameters using measurements from the Global Weather Observation (GWO) dataset provided by the British Atmospheric Data Center (BADC), and observed O_3 concentrations using the measurements included in AirBase, a European air quality database (EEA, 2017b). We then provided a more detailed analysis of the contribution of different source regions and types to MDA8 values describing total O_3 for the analysed period.

3.1 Evaluation of meteorology and chemistry

Since the accurate simulation of meteorological parameters represents a key factor affecting the concentrations of trace gases, we briefly compare the modelled mean sea level pressure (MSLP), 2 m temperature (T2M), 10 m wind speed (WS10M) and direction (WD10M) variables against GWO measurement. Predicted model variables were then evaluated against observations using statistical scores that include normalized mean bias (NMB), and the correlation factor between simulated and measured values (r).

An extensive evaluation of WRF-Chem using the MOZART chemical mechanism to predict long term meteorological data and O_3 levels has been presented previously (Mar et al., 2016). The main differences between the set-up used in this study and the model described by Mar et al. (2016) include differences between the versions of the model used (3.7.1 vs. 3.5.1, respectively), horizontal resolutions (50kmx50km vs. 45x45km, respectively), microphysics (Morrison vs. Lin, respectively) and cumulus schemes (Grell-Freitas vs. Grell 3-D, respectively), simulation years (2010 vs. 2007, respectively), anthropogenic emissions inventory (TNO-MACC III vs. TNO-MACC II, respectively), and chemical input and boundary conditions (extended CAM-Chem version 1.2 with MOZART-4 vs. MOZART-4/GEOS-5 simulations found at http://www.acom.ucar.edu/wrf-chem/mozart.shtm respectively).

Due to the coarse resolution of our domain, the air parcel dynamics associated with the complex topography of mountainous areas was not properly reproduced. Thus, we assessed the ability of the model to reproduce the meteorological variables using only those sites located below 1500 m above sea level. MSLP data were well reproduced over the entire period (NMB = 0 % and r = 0.98). The model predicted T2M values well (r = 0.91), however temperature was underestimated by 3 % (see Table 2). WS10M was also fairly well reproduced both in terms of spatial and temporal variability (NMB = 8 %, r = 0.63). Yet, WD10M data could not be predicted as well as other meteorological variables (NMB = 13 %, r = 0.47), behaviour could be related to the existence of unresolved topography features (Jimenez and Dudhia, 2012). However, the model performance is similar to Mar et al. (2016) and Tuccella et al. (2012).

We also compared modelled MDA8 O_3 concentrations with observations provided by the publicly-available AirBase dataset. The relatively coarse resolution of the domain may not be representative of changes in local emissions when the measurements are taken from urban areas; therefore, to aid in the analysis, we used only those stations characterized as rural. As can be seen in Table 3, evaluation of the model over entire period revealed that the model performs quite well with respect to the prediction of concentration and temporal evolution. Mar et al. (2016) reported a mean bias (MB) value of 15.85 μg m^{-3} and an NMB of 17% for the June–August 2007 period when the MOZART mechanism was used to assess the chemical performances of the model. For the same time period, we obtained an MB value of -5.92 μg m^{-3} and an NMB value of -6.3%. Tuccella et al. (2012) reported an annual MB of -1.4 μg m^{-3} when the RADM2 chemical mechanism was used to simulate a period throughout 2007. Month-to-month analysis (Table 3) shows that the model reproduces the O_3 concentration well compared to the Mar et al. (2016) and Tuccella et al. (2012). Even though the performance of the model in terms of temporal variation is relatively good (r values fall between 0.58 and 0.71), it mostly underestimated concentrations of O_3, except in September, when the model overestimated concentrations (NMB = 4.6%). Errors of the model may be explained by a wide range of uncertainties related

to modelled physical and chemical processes such as grid resolution, vertical and horizontal transport, boundary layer mixing, emission inventory, chemistry and photolysis rates, dry deposition, wet scavenging, etc. It is also possible that uncertainties in measurements contribute to observed errors. Since the focus of this study is on the contribution of different sources of precursors to the total tropospheric O_3 concentration of a particular area, a more thorough analysis of the ability of the model

5   to reproduce the observed meteorological variables is beyond the scope of this paper.

3.2   Contribution of tagged precursor sources to the MDA8 O_3 mixing ratios

Figure 2 shows the spatial distributions of simulated monthly mean MDA8 values from tagged O_3 source regions and other global source types throughout late spring in 2010. The receptor regions shown were mainly influenced by the overseas combination of NAM, ASI, OCN, and RST sources that combined contribute from 23 % in the Po Valley to up to 53.6 % in the

10   UKI region (see Table S1). O_3 from RST (a 7.5 - 15 % contribution) is the main source from overseas. O_3 from shipping NOx emissions advected through the model boundaries combined with O_3 produced from shipping NO_x emissions in the Atlantic Ocean mostly affects Atlantic coastal countries (up to a 16.1 % contribution in the UKI region), yet a small contribution of ~4-5 % was also observed within inland regions. Long-range transport of O_3 from Asia and North America contributes significantly to total observed O_3 in Europe, accounting for 9.6 % of the total observed O_3 in ITA and up to ~22 % in UKI and SCA. After

15   intercontinental transport, O_3 produced within Europe is an important source of O_3 in receptor regions, followed by O_3 coming from other global source types (LGT, BIO, and BMB). In general, for the April-May 2010 period, the contribution from the local sources to the total MDA8 O_3 mixing ratio in receptor regions falls within a range from 8.5 % (SCA) to 21 % (RBU) (see Table S1). Emissions from local sources do not only affect local O_3 mixing ratios, but also impact O_3 levels of bordering countries due to strong horizontal pollution transport. In all receptor regions, local anthropogenic sources have a lower contribution

20   to MDA8 O_3 mixing ratios than the sum of O_3 due to anthropogenic sources in other European source regions and long-range transport of ozone from intercontinental source regions. The contribution of intercontinental transport to the total MDA8 O_3 mixing ratio in Europe is consistent with previously reported results, i.e. Fiore et al. (2009) and Karamchandani et al. (2017), while this study allows us to identify which anthropogenic sources exert a strong influence on MDA8 O_3 predicted in different regions. Using observations, Danielsen (1968), Thouret et al. (2006) showed that the transport of O_3 from the stratosphere also

25   contributes to tropospheric O_3. Here, stratospheric O_3 contributes up to 7 ppb (12.5 % in SCA) to the total MDA8 O_3 mixing ratio, which is a finding similar to that reported by Derwent et al. (2015). A similar tagged system for predicting O_3 levels, using the CAM-Chem model (Butler et al., 2018), has also shown that stratospheric O_3 significantly contributes to the total tropospheric O_3 mixing ratio. The MOZART chemical mechanism used in this study does not explicitly treat stratospheric chemistry; thus surface stratospheric O_3 could be attributed to the vertical and horizontal transport of stratospheric O_3 and

30   stratospheric tagged precursors species concentrations coming from the CAM-Chem extended model that enters the domain through lateral boundaries.

During June-August 2010, Western Europe was mostly influenced by a high-pressure system centered over the Atlantic (see Fig. S1). In the upper troposphere, a ridge influenced the vertical atmospheric structure, especially over southern Europe. Therefore, these "usual summer conditions" favoured the intrusion of warm air coming from Africa and the Arabian peninsula

and led to a warm and dry climate characterized by subsidence, stability, clear skies and high-intensity solar radiation. Hence, the photochemical formation of O_3 was enhanced, and influenced the stronger contribution of local emissions to the total mixing ratio compared to the previous period examined. Figure 3 depicts the average MDA8 O_3 for June-August 2010. For most regions, we notice that levels of O_3 produced from local sources from June–August compared with April–May were

5   enhanced (Figure 2). Local sources can contribute to more than 20% of the mean MDA8 O_3 mixing ratio (from 14.6 % in SCA to 35.7 % in the Po Valley, see Table S1). This shows that local sources play a strong role in the formation of O_3 throughout the June-August period, as has been previously shown by Jiménez et al. (2006) and Querol et al. (2018). Compared with late spring, the relative contribution of overseas sources decreased in summer, varying from 10.9 % in the Po Valley receptor region to 44.8 % in the UKI region in the month of July (Figs. 2 and 3; Table S1). We noticed the spread of O_3 produced from

10   European anthropogenic precursors over bordering regions compared with late spring 2010 (Figs. 2 and 3). The increase in average temperature combined with stable atmospheric conditions lead to an enhancement of the biogenic NO emitted into the atmosphere, especially in South-Eastern and Eastern Europe; thus, the BIO global source type contributes up to ~9 ppb (13.2 % of MDA8 O_3) in the RBU receptor region (see Fig. 3). The vegetation fires that took place across Russia in July and August (Gilbert, 2010; Huijnen et al., 2012) as well as in Portugal and Spain (European Commission, 2011) lead to increases in the

15   contribution of O_3 coming from BMB of up to 29 ppb (16 %) in the RBU receptor region and up to 8.5 ppb (2.3 %) in the IBE receptor region. BMB emissions contribute domain-wide more than 3 % (Po Valley), with the greatest impacts modelled over RBU, IBA, SEE, SCA, and TCA. The enhanced photochemical activity during summer combined with the weakening of stratospheric-tropospheric exchange reduces the influence of stratospheric O_3 from a domain-wide mean MDA8 O_3 mixing ratio of 4.4 ppb in the spring to 1.3 ppb in the summer (Figs. 2 and 3).

20   The decrease in photochemical activity in September 2010 is reflected in decreases in total O_3 mixing ratios compared with the summer of the same year, as well as in a reduction associated with the local source contribution to the total O_3 mixing ratio (Fig. 4). Thus, only in IBE, TCA, FRA, Po Valley, the high Alps, and RBU regions was contribution of local sources to total MDA8 O_3 higher than 20 % (Table S1). On the other hand, we noticed an increase in O_3 coming from anthropogenic overseas sources and from lightning in autumn, stressing that seasonal variations exist within the outflow from other continents. There

25   also is variation in the lifetime of O_3 which is shortest during the summer as a result of enhanced photolytic activity.

Although we have seen that long-range transport plays a major role in total O_3 mixing ratios, the tagging technique helps to gain more insight into which region of the world dominates these mixing ratios in spring or autumn. In early fall, the Western European receptor regions exhibit a slight increase of 1.6 % in O_3 mixing ratios coming from North America compared with spring, while the contribution of O_3 mixing ratios coming from other overseas sources decreases. This could be linked to the

30   prevailing westerly wind and the synoptic conditions seen during the first period of September, when the Azores High extended far to the east and north (Fig S1). This phenomenon creates conditions that are conducive to the transatlantic transport of American pollution in the eastern direction. For example, in autumn periods within the RBU receptor region, North-American and oceanic sources account for up to 14.6 % in spring and 11.4 % in autumn of the MDA8 O_3 mixing ratios.

Apart from local and other global souce types, NO_x emissions from shipping activities in the Atlantic Ocean combined

35   with the oceanic O_3 from boundary conditions are an important source of O_3 that explains up to 16 % in late spring, 21% in

summer and 12% in early autumn of the MDA8 O_3 mixing ratio in the UKI, IBE, FRA, GEN, CEE, and SCA regions. Butler et al. (2018) showed that O_3 from oceanic sources reaches a minimum level in the North Atlantic Ocean during the summer, yet this study shows that in the UKI, IBE, FRA, GEN, CEE, and SCA receptor regions the oceanic O_3 contribution peaks in the summer. This implies that the nearby shipping emissions have a greater impact on oceanic bordering countries rather than oceanic O_3 from boundary conditions. Furthermore, the NO_x emissions from shipping activities in the Mediterranean and Black Seas account for up to 14 % in late spring, 19 % in summer and 11 % in early autumn of the MDA8 O_3 mixing ratio predicted in the receptor regions situated along the shore of the Mediterranean Sea, such as IBE, ITA, SEE, and FRA.

Our model results has shown that the highest MDA8 O_3 mixing ratios are predicted to occur over the Mediterranean Basin. This is due to the presence of favorable conditions for O_3 formation including the presence of small deposition sinks and intense photochemistry (Figs. 2–4). Several studies, such as Safieddine et al. (2014), Tagaris et al. (2017), Mertens et al. (2018), Querol et al. (2018) and the references therein, have used source attribution methods to establish the origin of tropospheric O_3 observed over the Mediterranean Basin. The tagging technique used here shows that the O_3 from shipping activities in the Mediterranean and Black Seas (MBS) explains, on average, 15 % in late spring, 20 % in summer and 12 % in early autumn of total MDA8 O_3 predicted to accumulate within the MBS receptor region. These findings are similar to those of Aksoyoglu et al. (2016) that showed these emissions accounted for 10-20 % of the mean O_3 in the Mediterranean in the summer of 2006. Moreover, Tagaris et al. (2017) have shown that shipping emissions explain up to 30 % the MDA8 O_3 simulated for July 2006 over the Mediterranean Sea. This study has shown that the shipping activities likely accounted for up to 35 % of the MDA8 O_3 near the Strait of Gibraltar (see Figure 5) during the April-September 2010 period. Shipping emissions contribute most highly to total O_3 in the Western Basin of the Mediterranean Sea. Aside from shipping activities, the other European source regions have a localized contribution to total MDA8 O_3 predicted in the Mediterranean Sea. Thus, ITA, ALP, GEN source regions contribute mostly to the central basin; IBE and FRA are main contributors in the western basin and SEE and TCA predominantly contribute to the eastern basin. Natural sources contribute on average up to 10% of MDA8 O_3 in the western basin, and up to approximately 25 % of MDA8 O_3 in the eastern basin. The long-range of O_3 transport contributes up to 45 % along the North African shore and it exhibits a zonal pattern, with low mixing ratios occurring in the North and high mixing ratios occurring south of the Mediterranean Sea, a trend mostly due to O_3 mixing ratios from NAF and RST sources.

3.3 Tagged ozone precursor contributions to exceedances of MDA8 target values – case study

As previously mentioned, the European Air Quality Directive (EU directive 2008/50/EC, 2008) has defined a target value of 120 μg m^{-3} for the MDA8 O_3 concentration, which can be exceeded up to 25 days per calendar year (over a three-year span). In the following, we refer to values that surpass 120 μg m^{-3} as exceedances, and values below 120 μg m^{-3} as non-exceedances. Figure S2 shows the spatial distribution of the number of exceedances observed and calculated throughout the April-September 2010 period for the AirBase rural stations. The observed MDA8 O_3 exceeds the target limits locally in Po Valley, Austria, and Germany; in coastal areas of Portugal, Spain, France and Italy; and inland areas of Poland and Slovakia. However, the modelled exceedances do not exhibit the same spatial pattern or intensity as observed values. Our use of tags allows for the identification of main source contributors to exceedances of modelled MDA8 O_3. Given the high number of

stations that measure O_3, for simplicity, we will discuss the source contribution to the MDA8 O_3 exceedances only for the Po Valley, high Alps, and GEN receptor regions.

Figure 6 exhibits the contribution of each tagged source and type to modelled and to observed MDA8 O_3 values. Samples were, in all cases, taken at the location of the measurement stations, throughout the April-September 2010 period. Figure 6 shows the average conditions during the exceedance of the MDA8 O_3 target value, and also, at times, occurred when the target value was not exceeded. To perform the source attribution for the observed values, we have scaled these values proportionally by the relative concentrations of each tagged O_3 tracer in our model output.

The relative contribution of emissions from different source regions to modelled and to observed MDA8 O_3 values, after being scaled to account for the contribution of modelled sources of O_3 types is generally similar for Po Valley and GEN receptor regions (see Fig. 6). In the Po Valley, we can pinpoint the main remote contributor as being MBS (see Fig. 6), followed by GEN, and FRA, suggesting a dominant westerly and northerly air flow. The recirculation of air masses in the Gulf of Genoa could accentuate the sea breeze and therefore more O_3 coming from NO_x associated with shipping activities in the Mediterranean will be transported to the coastal and inland station.

The high Alps receptor region is less influenced by ALP emissions than the Po Valley, and is more influenced by remote sources (see Fig. 6). The increased contribution of O_3 from CEE, ITA and FRA to both exceedance and non-exceedance days in the high Alps receptor region compared with the Po Valley receptor region highlights the impact of the transboundary transport of O_3 and its precursors . Furthermore, the contribution of stratospheric as well as long-range sources was generally 6 % higher in this receptor region than in the Po Valley receptor region.

In GEN, the main remote source regions are FRA and CEE during the exceedance days and FRA and UKI during non-exceedance days (Fig. 6). Opposite to Po Valley, in GEN the model predicts fewer MDA8 O_3 exceedances days. Comparing the source contribution to both modelled and observed exceedances days, we noticed that the model underestimates O_3 concentrations associated with long-range transport and natural sources. Further, the model predicted higher levels of O_3 from CEE and FRA than observed. Underestimation of long-range transported O_3 into the GEN region in our model could be explained by the fact that the number of modelled MDA8 O_3 exceedances in GEN is half of the observed number of exceedances (Fig. 6).

This kind of analysis can be applied to improve our knowledge of the origin of O_3 precursors and their contribution to MDA8 O_3 health metrics. Hence, by using this tagging technique, policymakers can identify future actions required to control the NO_x emissions at local and regional levels.

3.4 Tagged ozone precursor contributions to regulatory ozone metrics

In this section, we discuss the contribution of O_3 mixing ratios from diverse emissions sources and types to several metrics that quantify the O_3 exposures of humans and ecosystems. From modelled hourly mixing ratios of tagged O_3 sources and other global types, we have calculated different O_3 metrics, including non-cumulative (mean, MDA8, and the 95th percentile O_3) and cumulative (SOMO35, W126, and AOT40) metrics. We have chosen not to analyse the performance of the calculated cumulative metrics in comparison with measured values, as was done in previous work by Tong et al. (2009). Their work

showed that the poor performance of the cumulative metrics is closely related to the sensitivity of these metrics to the threshold values or weighting factors.

Figure 7 and Table S2 include the percentage of the contribution of different sources of emissions and other global types to total O_3 as calculated using health and vegetation metrics. The non-cumulative O_3 metrics employed in this study have displayed similar patterns for most of the receptor regions. The contribution of local and European sources to the total O_3 mixing ratios have been low when we applied to mean O_3 metric and high when using 95th percentile metric. These findings emphasize the importance of O_3 produced by local and neighbouring sources to the high end of the O_3 mixing ratio distribution.

Splitting the non-cumulative metrics into early (April-June) and late (July-September) simulation periods clearly illustrates that the European receptor regions are more prone to be influenced by intercontinental transport during the early period than the late period. The contribution of intercontinentally transported O_3 to mean O_3 values in different receptor regions is higher during the early period and it spans between 22.8 % and 54.3 % of total O_3. In the late period it accounts for between 16 % and 48.9 % of total O_3 (see Fig. 7 and Table S2). Since O_3 associated with intercontinental transport comes, in this case, solely from boundary conditions, errors in boundary conditions affect the predicted mixing ratio of various chemical species, and, consequently, the contribution of overseas sources of O_3 to levels observed in Europe O_3 (Tang et al., 2007; Giordano et al., 2015; Im et al., 2018).

The shorter lifespan of O_3 over remote ocean regions throughout the warm season, combined with synoptic conditions, has led to decreased levels of intercontinentally transported O_3 to Europe. Thus, for most receptor regions, the O_3 coming from Asia and the rest of the world was reduced by more than half when compared with the cold period. The O_3 mixing ratio from the stratosphere is, in general, 2.5 times higher in the cold season than in the warm season which is consistent with the findings of a study by Butler et al. (2018) which showed that the stratospheric O_3 mixing ratio varies with altitude and its lifetime is influenced by season and latitude. The tagging technique also helps to quantify the impact of biogenic and biomass burning emissions of NO_x on tropospheric O_3. The impact of biogenic NO_x emissions on mean O_3 mixing ratios is between 3.3 % in Po Valley and 5.9 % in TCA in the early season, while during the late season it is between 5.4 % in Po Valley and 13.4 % in RBU. The biomass burning emissions account for variable percentages of mean O_3 mixing ratios. These span between 1.6 % in ITA to 5.3 % in RBU during the early season, and between 3.8 % in Po Valley and 16.3 % in RBU during the late season. Natural sources do not usually vary greatly when different non-cumulative metrics are applied. An exception would be for the biomass burning emissions on RBU during the late season. Thus, BMB in RBU contributes to 16.3 %, 17.6 % and 28.8 % of the mean, MDA8 and 95th percentile, respectively.

Even though the SOMO35 and AOT40 metrics are not accumulated over the same period (SOMO35 is accumulated over the entire simulated period, and AOT40 metric is accumulated over the May-July period) and do not use same input data (daily MDA8 O_3 for SOMO35 vs daytime O_3 mixing ratios for AOT40), since they are based on threshold exceedances and are designed to measure exposure to high O_3 levels of humans (SOMO35) and vegetation (AOT40), there is a way to directly compare data from each metric type. As shown in Figure 7 and Table S2, the contribution of different sources of emissions and types as a proportion of total SOMO35 and AOT40 metrics is similar for most of the European receptor regions. Their spatial distribution (not shown) is also comparable, with minimum values over the UK, NW Europe and Scandinavia and maximum

values over Italy, the Alps, south of Spain, east of Turkey and in the metropolitan area of Moscow, Russia. These results are consistent with previous studies performed by Aksoyoglu et al. (2014), and Anav et al. (2016). The overseas sources contribute similarly to SOMO35 and AOT40 indexes (usually less than 30 %) for most of the receptor regions used in this study. However, in UKI the overseas sources account for 32 % of AOT40 and 38 % of SOMO35, and in SCA they contribute to ~22 % of AOT40 and 30 % of SOMO35. This suggests that these metrics are more sensitive with respect to the O_3 mixing ratios from remote sources in areas having a low level of O_3 pollution. In the RBU receptor region, these indicators are sensitive to O_3 coming from biomass burning emissions (20 % of SOMO35 and 24 % of AOT40), whereas for the remaining receptor regions the contribution of natural sources to SOMO35 and AOT40 is similar. Local sources account for a range of ~12 % (SCA) to ~38 % (GEN) of these metrics. These data highlight the occurrence of increased O_3 production from local sources in comparison with northern European countries as well as large emissions of NO_x in the GEN source region. Since the difference between AOT40 and SOMO35 is only a few percentage points, regardless of the receptor region, we were able to conclude that they behave similarly, according to thresholds used to define these metrics.

The tagging method allows a better understanding of the main precursor sources responsible for exceedances of regulatory O_3 metrics. This information can help to inform further modelling studies aimed at investigating the effects of emission reduction strategies, and ultimately inform air quality policy. For example, in the Po Valley receptor region, the modelled AOT40 is up to 3.4 times higher than the target limit given by EU legislation (on average 31218 $\mathrm{ppb-hours}$). The observed and calculated AOT40 values depicted in Figure S3 exhibit the exceedance of target limits in Po Valley. O_3 coming from local sources can explain 35.0 % of this value (an average of 10909 $\mathrm{ppb-hours}$). After local sources, the main European anthropogenic sources contributing to high AOT40 values in the Po Valley region are from FRA (6.6 %), GEN (7 %) and MBS (8.8 %) (Table S2). Generally, the O_3 mixing ratio and its precursors transported from other anthropogenic European sources into the Po Valley receptor regions account for ~39.5 %, while natural sources account for ~12.3 % and long-range transport accounts for ~13.4 % of the remaining AOT40 mixing ratios. Thus, to reach at least the target limit in the Po Valley receptor region, considerable emission reductions will still be needed, not only on a local scale but also on the European scale, especially within the MBS, GER, and FRA source regions.

Figure 7 also shows the percentage that different types of emissions and emission regions contribute to the W126 index. Interestingly, for most of the receptor regions, local NO_x anthropogenic emissions cause the largest response in W126 values compared with the other cumulative metrics used in this study. Thus, local NO_x explains from 10.9 % (0.1 $\mathrm{ppm-hours}$) in SCA to more than 40 % of W126 in GEN (45.9 %; 2.48 $\mathrm{ppm-hours}$, and Po Valley (45.4 %; 8.7 $\mathrm{ppm-hours}$) of W126 index values calculated for each region. The effect of European transported plumes is also enhanced when using the W126 index compared with the other metrics for most of the downwind receptor regions. This behaviour is related to how these metrics have been defined. Due to its sigmoidal weighted formulation, as discussed in Westenbarger and Frisvold (1995), and Lapina et al. (2014), W126 includes all daytime values rather than O_3 levels above a certain threshold, as is done using SOMO35 and AOT40; therefore lower weighting factors of less than 0.5 are given to low O_3 values and weighting factors above 0.5 are given to O_3 values situated above the inflection point of 67 ppb.

The modelled mean AOT40 and W126 values in the Po Valley receptor region exceeded standards (26368 $ppb-hours$ for AOT40 and 28.9 $ppm-hours$ for W126) during the May-July 2010 period, and, as shown in Fig. 7 and Table S2, local sources are an important contributor to these metrics. To better understand why the W126 index is mainly influenced by local sources compared with the other cumulative metrics, we thoroughly compared AOT40 and W126 values for the Po Valley receptor region. As shown in Figure 8, a temporal series of hourly daylight values for mean O_3, W126 and AOT40 values averaged over the Po Valley receptor region are given. Since the W126 unit is $ppm-hours$, a more direct comparison with the W126 index would require values be expressed in $ppb-hours$. Further, all metrics showed a similar level of temporal variation in which they peaked in the first half of July. Also, whenever the averaged O_3 mixing ratio was lower than 60 ppb (Fig. 8a), W126 value was lower than AOT40 (Fig. 8d). This way of acting was most probably due to the weighting factor being less than 0.3, and above this mixing ratio W126 tends to be higher than AOT40. This behaviour is closely linked to the definition of these metrics. If the O_3 mixing ratio is less than 40 ppb, W126 has a weighting factor lower than 0.03, while AOT40 has a weighting factor of 0. Above this threshold, AOT40 has a weighting factor of 1, while in the case of W126 only O_3 values higher than 100 ppb have a weighting factor of 1. Due to the way these metrics are defined, predicted O_3 values in each grid cell are accounted for the W126, may not be accounted for the AOT40 index.

In addition, visual analysis of the time series also revealed that when the O_3 mixing ratios from local sources are ~20 ppb, these mixing ratios have a higher contribution to W126 than AOT40. To better understand this observation, we have further analysed the relationship between mean O_3 values from ALP sources (O_3-ALP) and the percent contribution of these O_3 tracers to mean O_3, W126, and AOT40 metrics. Figure 9 shows scatter plots for O_3-ALP that relate the contributions of these mixing ratios on mean O_3, W126, and AOT40. In addition, the linear regressions of Y vs X (Y=a*X+b) using all data sets have been applied. We saw that in general, high mean O_3-ALP mixing ratios have a higher contribution to W126 than to AOT40; this was also confirmed by the linear regression between O_3-ALP and W126 that yields a slope of 1.52 compared to a slope of 1.36 obtained when the linear regression was applied to AOT40 vs. O_3-ALP. Averaged O_3-ALP and mean O_3 as well as O_3-ALP and W126 were highly correlated (r=0.96, and r=0.93,respectively), while O_3-ALP and AOT40 are correlated more loosely (0.88). The high level of correlation between O_3-ALP and both mean O_3 and W126 could be related to the fact that these metrics account for all modelled values, whilst AOT40 considers only O_3 values above 40 ppb.

Extending this analysis to all receptor regions, we can explain why the W126 index is more sensitive to O_3 coming from local sources compared with the other cumulative metrics. In addition, W126 accentuates the contribution of BIO and BMB in RBU, TCA and SEE, most likely because the metric includes all daytime values, and not just those above a certain threshold. Thus, the use of W126 highlights the considerable impacts of BIO and BMB emissions on total O_3 mixing ratios throughout the summer and from burning vegetation that ultimately influence the extent to which O_3 causes damage to vegetation.

We have seen that the contribution of NO_x to total O_3 varies depending on metrics and regions considered. Hence, the tagging method could help design different emission control strategies in specific source regions depending on which impacts need to be reduced in specific receptor regions.

4 Conclusions

Here, we implemented a new chemical mechanism within the WRF-Chem model to account for source attribution of O_3 from NO_x. We investigated the origin of surface O_3 using the "tagging" technique from April-September 2010, as well as the contribution of different sources to O_3 metrics, and their exceedance events.

Using tagged simulation from WRF-Chem, we show that the spatial distribution of simulated monthly mean MDA8 from tagged O_3 source regions and other global types throughout late spring, summer and early autumn of 2010. The contribution of different sources to O_3 production varies with season. We have identified intercontinental transported O_3 as an important contributor to the total O_3 mixing ratio, especially in the late spring and early autumn. During summer, however, the O_3 production is dominated by national and intra-European sources. We have also identified shipping activities in the Mediterranean Sea as an important source of O_3 for the IBE, ITA, SEE, and FRA peripheral maritime receptor regions. We also analysed the main sources of MDA8 O_3 over the Mediterranean Basin and we have identified the main factors that contribute to MDA8 O_3 mixing ratios to the greatest degree. These were mainly shipping activities and the localized contribution from the bordering countries.

To better understand the origin of MDA8 O_3 exceedances, we compared modelled and observed values of MDA8 O_3 concentration in the Po Valley, high Alps, Germany, and Benelux receptor regions. Throughout days exceeding the recommended thresholds of 120 μg, the contribution from local sources was ~41 %, 34 % and 38 % of modelled MDA8 O_3 for Po Valley, high Alps, and GEN, respectively. Throughout days not exceeding recommended thresholds, local emissions explain ~27 %, 16 % and 23% of modelled MDA8 O_3 for the Po Valley, high Alps, and GEN, respectively. Moreover, this tagging approach revealed that the main remote sources of MDA8 O_3 are MBS, GEN, and FRA for the Po Valley receptor region, and are FRA, CEE and UKI for Germany and Benelux receptor region. In addition, these analyses identified a persistently high contribution of transboundary sources to background O_3 concentration in the high Alps receptor region. Furthermore, by showing that the contribution of precursor sources to modelled O_3 target value exceedances in the GEN region is systematically different from the contribution of precursor sources to modelled O_3 when exceedances are observed but not modelled, we have identified a possible reason (underestimation of long-range transport) for the poor performance of our model with respect to reproducing the observed number of O_3 target value exceedances in the GEN region.

Through comparisons with different O_3 metrics, we quantified the impact of local vs. non-local NO_x on O_3 production for each European receptor region. The comparison between mean, MDA8 and 95th percentile O_3 metrics accentuate the importance of large contributions from different NO_x to the high-end of the O_3 distribution. By analysing these metrics for two periods (April-June and July-September), we can clearly distinguish the contribution of different NO_x to total O_3 mixing ratios in each region and throughout different times of the year. When we compare the cumulative metrics, we noticed that the SOMO35 and AOT40 indexes exhibit rather similar behaviour. Considering that these metrics are not calculated over the same period nor do they use same input data, the similar behaviour is likely due to the similar threshold values applied to define these metrics.

The use of the W126 index accentuates the importance of local emissions. To confirm this, we investigated the behaviour of modelled mean AOT40 and W126 values in the Po Valley receptor region. We noticed that when the local sources contribute to more than 20 ppb of the O_3 mixing ratios, these mixing ratios have a higher contribution to W126 than they do to AOT40 and determined that the difference was mostly due to the definition of W126 which takes into account all O_3 values, not only those that are above a certain threshold.

Overall, this study has identified local and remote factors that contribute to the MDA8 O_3 mixing ratio during several periods as well as within different O_3 metrics. Furthermore, the method applied here could be used to design improved emission control strategies depending on which impacts need to be reduced.

Appendix A

– chemics_init.F;

– module_input_chem_data.F;

– module_plumerise1.F and module_add_emiss_burn.F to account the source attribution of biomass burning emissions to O_3 concentration;

– module_emissions_anthropogenics.F to account for the impact of anthropogenic emissions on O_3 concentration;

– module_bioemi_megan2.F and module_data_mgn2mech.F to see the impact of biogenic emissions on O_3 concentration;

– module_lightning_nox_driver.F for lightning-generated nitrogen oxides

– Dry and wet deposition of tagged trace gases are treated by module_dep_simple.F and module_mozcart_wetscav.F, thus all tagged species have the same dry deposition velocities and wet removal rates with the corresponding non-tagged species;

– module_ftuv_driver.F to consider the photolytical reaction of the new packages;

– emissions_driver.F;

– chem_driver.F.

Code and data availability. The WRF-Chem model is publicly available on http://www2. mmm.ucar.edu/wrf/users/download/get_source.html. The modification introduced and described in Section 2 as well as the model data can be provided upon request to the corresponding author.

Author contributions. AL and TB designed the research. AL adapted the automatic mechanism-rewriting and code-generation tools and in implemented into WRF-Chem source code. AL performed the model runs and subsequent analysis. AL wrote the pape with contribution from TB.

5 *Acknowledgements.* This work was hosted by IASS Potsdam, with financial support provided by the Federal Ministry of Education and Research of Germany (fBMBF) and the Ministry for Science, Research and Culture of the State of Brandenburg (MWFK). The authors would like to thank Kathleen Mar for helping with the emissions preprocessing as well as to Jane Coates for her help with some of the plots.

References

Agathokleous, E., Kitao, M., and Kinose, Y. .: A Review Study on Ozone Phytotoxicity Metrics for Setting Critical Levels in Asia, Asian Journal of Atmospheric Environment, 12, 1–16, https://doi.org/https://doi.org/10.5572/ajae.2018.12.1.001, 2018.

Aksoyoglu, S., Keller, J., Ciarelli, G., Prévôt, A. S. H., and Baltensperger, U.: A model study on changes of European and Swiss particulate matter, ozone and nitrogen deposition between 1990 and 2020 due to the revised Gothenburg protocol, Atmos. Chem. Phys., 14, 13 081–13 095, https://doi.org/https://doi.org/10.5194/acp-14-13081-2014, 2014.

Aksoyoglu, S., Baltensperger, U., and Prévôt, A. S. H.: Contribution of ship emissions to the concentration and deposition of air pollutants in Europe, Atmos. Chem. Phys., 16, 1895–1906, https://doi.org/https://doi.org/10.5194/acp-16-1895-2016, 2016.

Anav, A., De Marco, A., Proietti, C., Alessandri, A., Dell'Aquila, A., Cionni, I., Friedlingstein, P., Khvorostyanov, D., Menut, L., Paoletti, E., Sicard, P., Sitch, S., Vitale, M., Anav, A., De Marco, A., and Proietti, C.: Comparing concentration-based (AOT40) and stomatal uptake (PODY) metrics for ozone risk assessment to European forests, Global Change Biology (2016), 22, 1608–1627, https://doi.org/10.1111/gcb.13138, 2016.

Avnery, S., Mauzerall, D. L., L, D., and Fiore, A. M.: Increasing global agricultural production by reducing ozone damages via methane emission controls and ozone-resistant cultivar selection, Glob. Change Biol., 19, 1285–1299, https://doi.org/10.1111/Gcb.12118, 2013.

Butler, T., Lupascu, A., Coates, J. a., and Zhu, S.: TOAST 1.0: Tropospheric Ozone Attribution of Sources with Tagging for CESM 1.2.2, Geosci. Model Dev., 11, 2825–2840, https://doi.org/https://doi.org/10.5194/gmd-11-2825-2018, 2018.

Chan, C. K. and Yao, X.: Air pollution in mega cities in China, Atmos. Environ., 42, 1–42, https://doi.org/10.1016/j.atmosenv.2007.09.003, 2008.

Chou, M.-D. and Suarez, M. J.: An efficient thermal infrared radiation parametrization for use in general circulation models, NASA Tech. Memo., 104606, 85 pp, 1994.

Christensen, J. H. and Christensen, O. B.: A summary of the PRUDENCE model projections of changes in European climate by the end of this century, Climatic Change, 81(Suppl 1): 7, https://doi.org/doi:10. 1007/s10584-006-9210-7, 2007.

Colette, A., Granier, C., Hodnebrog, ., Jakobs, H., Maurizi, A., Nyiri, A., Rao, S., Amann, M., Bessagnet, B., D'Angiola, A., Gauss, M., Heyes, C., Klimont, Z., Meleux, F., Memmesheimer, M., Mieville, A., Rouïl, L., Russo, F., Schucht, S., Simpson, D., Stordal, F., Tampieri, F., and Vrac, M.: Future air quality in Europe: a multi-model assessment of projected exposure to ozone, Atmos. Chem. Phys., 12, 10 613–10 630, https://doi.org/10.5194/acp-12-10613-2012, 2012.

Dahlmann, K., Grewe, V., Ponater, M., and Matthes, S.: Quantifying the contributions of individual NOx sources to the trend in ozone radiative forcing, Atmos. Environ., 45, 2860–2868, https://doi.org/10.1016/j.atmosenv.2011.02.071, 2011.

Danielsen, E. F.: Stratospheric-tropospheric exchange based on radioactivity ozone and potential vorticity, J. Atmos. Sci., 2, 502–518, https://doi.org/https://doi.org/10.1175/1520-0469(1968)025<0502:STEBOR>2.0.CO;2, 1968.

Derwent, R. G., Utember, S. R., Jenkin, M. E., and Shallcross, D. E.: Tropospheric ozone production regions and the intercontinental origins of surface ozone over Europe, Atmos. Environ., p. 216–224, 2015.

EEA: Air quality in Europe-2017 report, EEA Report, No 13/2017,ISBN 978-92-9213-920-9, Luxembourg: Publications Office ofthe European Union, available at: https://www.eea.europa.eu/publications/air-quality-in-europe-2017, (last access:26 June 2019), 80 pp., 2017a.

EEA: AirBAse - The European air quality database, available at: https://www.eea.europa.eu/data-and-maps/data/aqereporting-8, (last access: 12 September 2018), 2017b.

Emmons, L. K., Hess, P. G., Lamarque, J.-F., and Pfister, G. G.: Tagged ozone mechanism for MOZART-4, CAM-chem and other chemical transport models, Geoscientific Model Development, 5, 1531–1542, https://doi.org/10.5194/gmd-5-1531-2012, https://www.geosci-model-dev.net/5/1531/2012/, 2012.

EU directive 2008/50/EC: EU directive 2008/50/EC of the European parliament and of the council on Ambient Air Quality and Cleaner Air for Europe (http://eur-lex.europa.eu/LexUriServ/LexUriServ.do?uri=OJ:L:2008:152:0001:0044:en:PDFm, last accessed April 6, 2018), 2008.

European Commission: Forest Fires in Europe 2010, Luxembourg: Publications Office of the European Union, EUR 24910 EN, ISBN 978-92-79-20919-2, 2011.

Fiore, A., Dentener, F. J., Wild, O., Cuvelier, C., Schultz, M. G., Hess, P., Textor, C., Schulz, M., Doherty, R. M., Horowitz, L. W., MacKenzie, I. A., Sanderson, M. G., Shindell, D. T., Stevenson, D. S., Szopa, S., Dingenen, R. V., Zeng, G., Atherton, C., Bergmann, D., Bey, I., Carmichael, G., Collins, W. J., Duncan, B. N., Faluvegi, G., Folberth, G., Gauss, M., Gong, S., Hauglustaine, D., Holloway, T., Isaksen, I. S. A., Jacob, D. J., Jonson, J. E., Kaminski, J. W., Keating, T. J., Lupu, A., Marmer, E., Montanaro, V., Park, R. J., Pitari, G., Pringle, K. J., Pyle, J. A., Schroeder, S., Vivanco, M. G., Wind, P., Wojcik, G., Wu, S., and Zuber, A.: Multimodel estimates of intercontinental source-receptor relationships for ozone pollution, Journal of Geophysical Research: Atmospheres, 114, https://doi.org/10.1029/2008JD010816, 2009.

Fleming, Z., Doherty, R., Von Schneidemesser, E., Malley, C., Cooper, O., Pinto, J., Colette, A., Xu, X., Simpson, D., Schultz, M., Lefohn, A., Hamad, S., Moolla, R., Solberg, S., and Feng, Z.: Tropospheric Ozone Assessment Report: Present-day ozone distribution and trends relevant to human health, Elementa, 6, https://doi.org/10.1525/elementa.273, 2018.

Flemming, J., Huijnen, V., Arteta, J., Bechtold, P., Beljaars, A., Blechschmidt, A.-M., Diamantakis, M., Engelen, R. J., Gaudel, A., Inness, A., Jones, L., Josse, B., Katragkou, E., Marecal, V., Peuch, V.-H., Richter, A., Schultz, M. G., Stein, O., and Tsikerdekis, A.: Tropospheric chemistry in the Integrated Forecasting System of ECMWF, Geoscientific Model Development, 8, 975–1003, https://doi.org/10.5194/gmd-8-975-2015, https://www.geosci-model-dev.net/8/975/2015/, 2015.

Folberth, G. A., Butler, T. M., Collins, W. J., and Rumbold, S. T.: Megacities and climate change – A brief overview, Environmental Pollution, 203, 235 – 242, https://doi.org/https://doi.org/10.1016/j.envpol.2014.09.004, 2015.

Gao, J., Zhu, B., Xiao, H., Kang, H., Hou, X., and Shao, P.: A case study of surface ozone source apportionment during a high concentration episode, under frequent shifting wind conditions over the Yangtze River Delta, China, Science of the Total Environment, 544, 853–863, https://doi.org/http://dx.doi.org/10.1016/j.scitotenv.2015.12.039, 2016.

Gaudel, A., Cooper, O. R., Ancellet, G., Barret, B., Boynard, A., Burrows, J. P., Clerbaux, C., Coheur, P. ., Cuesta, J., Cuevas, E., Doniki, S., Dufour, G., Ebojie, F., Foret, G., Garcia, O., Granados-Muñoz, M. J., Hannigan, J. W., Hase, F., Hassler, B., Huang, G., Hurtmans, D., Jaffe, D., Jones, N., Kalabokas, P., Kerridge, B., Kulawik, S., Latter, B., Leblanc, T., Le Flochmoën, E., Lin, W., Liu, J., Liu, X., Mahieu, E., McClure-Begley, A., Neu, J. L., Osman, M., Palm, M., Petetin, H., Petropavlovskikh, I., Querel, R., Rahpoe, N., Rozanov, A., Schultz, M. G., Schwab, J., Siddans, R., Smale, D., Steinbacher, M., Tanimoto, H., Tarasick, D. W., Thouret, V., Thompson, A. M., Trickl, T., Weatherhead, E., Wespes, C., Worden, H. M., Vigouroux, C., Xu, X., Zeng, G., and Ziemke, J.: Tropospheric Ozone Assessment Report: Present-day distribution and trends of tropospheric ozone relevant to climate and global atmospheric chemistry model evaluation, Elementa, 6, p. 39, https://doi.org/http://doi.org/10.1525/elementa.291, 2018.

Gilbert, N.: Russia counts environmental cost of wildfires, Nature News, https://doi.org/doi:10.1038/news.2010.404, 2010.

Giordano, L., Brunner, D., Flemming, J., Hogrefe, C., Im, U., Bianconi, R., Badia, A., Balzarini, A., Baro, R., Chemel, C., Curci, G., Forkel, R., Jimenez-Guerrero, P., Hirtl, M., Hodzic, A., Honzak, L., Jorba, O., Knote, C., Kuenen, J. J. P., Makar, P. A., Manders-Groot, A., Neal,

L., Perez, J. L., Pirovano, G., Pouliot, G., San Jose, R., Savage, N., Schroder, W., Sokhi, R. S., Syrakov, D., Torian, A., Tuccella, P., Werhahn, J., Wolke, R., Yahya, K., Žabkar, R., Zhang, Y., and Galmarini, S.: Assessment of the MACC re-analysis and its influence as chemical boundary conditions for regional air quality modeling in AQMEII-2, Atmos. Environ., 115, 371–388, 2015.

Grell, G. A. and Freitas, S. R.: A scale and aerosol aware stochastic convective parameterization for weather and air quality modeling, Atmospheric Chemistry and Physics, 14, 5233–5250, https://doi.org/10.5194/acp-14-5233-2014, https://www.atmos-chem-phys.net/14/5233/2014/, 2014.

Grell, G. A., Peckham, S. E., Schmitz, R., McKeen, S. A., Frost, G., Skamarock, W. C., and Eder, B.: Fully coupled online chemistry within the WRF model, Atmos. Environ., 39, 6957–6975, 2005.

Grewe, V., Tsati, E., and Hoor, P.: On the attribution of contributions of atmospheric trace gases to emissions in atmospheric model applications, Geoscientific Model Development, 3, 487–499, https://doi.org/10.5194/gmd-3-487-2010, https://www.geosci-model-dev.net/3/487/2010/, 2010.

Grewe, V., Dahlmann, K., Matthes, S., and Steinbrecht, W.: Attributing ozone to NOx emissions: Implications for climate mitigation measures, Atmos. Environ., 59, 102–107, https://doi.org/doi:10.1016/j.atmosenv.2012.05.002:, 2012.

Grewe, V., Tsati, E., Mertens, M., Fromming, C., and Jockel, P.: Contribution of emissions to concentrations: the TAGGING 1.0 submodel based on the Modular Earth Submodel System (MESSy 2.52), Geoscientific Model Development, 10, 2615–2633, https://doi.org/10.5194/gmd-10-2615-2017, https://www.geosci-model-dev.net/10/2615/2017/, 2017.

Gromov, S., Jöckel, P., Sander, R., and Brenninkmeijer, C. A. M.: A kinetic chemistry tagging technique and its application to modelling the stable isotopic composition of atmospheric trace gases, Geoscientific Model Development, 3, 337–364, https://doi.org/10.5194/gmd-3-337-2010, https://www.geosci-model-dev.net/3/337/2010/, 2010.

Guenther, A., Karl, T., Harley, P., Wiedinmyer, C., Palmer, P. I., and Geron, C.: Estimates of global terrestrial isoprene emissions using MEGAN (Model of Emissions of Gases and Aerosols from Nature), Atmospheric Chemistry and Physics, 6, 3181–3210, https://doi.org/10.5194/acp-6-3181-2006, https://www.atmos-chem-phys.net/6/3181/2006/, 2006.

Hong, S.-Y., Noh, Y., and Dudhia, J.: A new vertical diffusion package with an explicit treatment of entrainment processes, Mon. Weather Rev., 134, 2318–2341, https://doi.org/10.1175/MWR3199.1, 2006.

HTAP: Hemispheric Transport of Air Pollution 2010, Part A: Ozone and Particulate Matter, Air Pollution Studies,No.17, Geneva, Switzerland, 2010.

Huijnen, V., Flemming, J., Kaiser, J. W., Inness, A., Leitão, J., Heil, A., Eskes, H. J., Schultz, M. G., Benedetti, A., Hadji-Lazaro, J., Dufour, G., and Eremenko, M.: Hindcast experiments of tropospheric composition during the summer 2010 fires over western Russia, Atmospheric Chemistry and Physics, 12, https://doi.org/10.5194/acp-12-4341-2012, https://www.atmos-chem-phys.net/12/4341/2012/, 2012.

Iacono, M., Delamere, J., Mlawer, E., Shephard, M., Clough, S., and Collins, W.: Radiative forcing by long-lived greenhouse gases: Calculations with the AER radiative transfer models, J. Geophys. Res.-Atmos., 113, https://doi.org/10.1029/2008JD009944, 2008.

Im, U., Christensen, J. H., Geels, C., Hansen, K. M., Brandt, J., Solazzo, E., Alyuz, U., Balzarini, A., Baro, R., Bellasio, R., Bianconi, R., Bieser, J., Colette, A., Curci, G., Farrow, A., Flemming, J., Fraser, A., Jimenez-Guerrero, P., Kitwiroon, N., Liu, P., Nopmongcol, U., Palacios-Peña, L., Pirovano, G., Pozzoli, L., Prank, M., Rose, R., Sokhi, R., Tuccella, P., Unal, A., Vivanco, M. G., Yarwood, G., Hogrefe, C., and Galmarini, S.: Influence of anthropogenic emissions and boundary conditions on multi-model simulations of major air pollutants over Europe and North America in the framework of AQMEII3, Atmospheric Chemistry and Physics, 18, 8929–8952, https://doi.org/10.5194/acp-18-8929-2018, https://www.atmos-chem-phys.net/18/8929/2018/, 2018.

Jimenez, P. A. and Dudhia, J.: Improving the Representation of Resolved and Unresolved Topographic Effects on Surface Wind in the WRF Model, J. Appl Meteor. and Climo, 51, 300–316, https://doi.org/https://doi.org/10.1175/JAMC-D-11-084.1, 2012.

Jiménez, P., Lelieveld, J., and Baldasano, J. M.: Multiscale modeling of air pollutants dynamics in the northwestern Mediterranean basin during a typical summertime episode, Journal of Geophysical Research: Atmospheres, 111, https://doi.org/10.1029/2005JD006516, 2006.

5   Jiménez, P., Dudhia, J., González-Rouco, J., Navarro, J., Montávez, J., and García-Bustamante, E.: A revised scheme for the WRF surface layer formulation, Mon. Weather Rev., 140, 898–918, https://doi.org/10.1175/MWR-D-11-00056.1, 2012.

Karamchandani, P., Long, Y., Pirovano, G., Balzarini, A., and Yarwood, G.: Source-sector contributions to European ozone and fine PM in 2010 using AQMEII modeling data, Atmospheric Chemistry and Physics, 17, 5643–5664, https://doi.org/10.5194/acp-17-5643-2017, https://www.atmos-chem-phys.net/17/5643/2017/, 2017.

10   Kuenen, J. J. P., Visschedijk, A. J. H., Jozwicka, M., and Denier van der Gon, H. A. C.: TNO-MACCII emission inventory; a multi-year (2003-2009) consistent high-resolution European emission inventory for air quality modelling, Atmospheric Chemistry and Physics, 14, 10 963–10 976, https://doi.org/10.5194/acp-14-10963-2014, https://www.atmos-chem-phys.net/14/10963/2014/, 2014.

Lapina, K., Henze, D. K., Milford, J. B., Huang, M., Lin, M., Fiore, A. M., Carmichael, G., Pfister, G. G., and Bowman, K.: Assessment of source contributions to seasonal vegetative exposure to ozone in the U.S., Journal of Geophysical Research: Atmospheres, 119, 324–340,

15   https://doi.org/10.1002/2013JD020905, 2014.

Lefohn, A., Malley, C., Smith, L., Wells, B., Hazucha, M., Simon, H., Naik, V., Mills, G., Schultz, M., Paoletti, E., De Marco, A., Xu, X., Zhang, L., Wang, T., Neufeld, H., Musselman, R., Tarasick, D., Brauer, M., Feng, Z., Tang, H., Kobayashi, K., Sicard, P., Solberg, S., and Gerosa, G.: Tropospheric ozone assessment report: Global ozone metrics for climate change, human health, and crop/ecosystem research, Elem Sci Anth, 6(1), 28, https://doi.org/https://doi.org/10.1525/elementa.279, 2018.

20   Lefohn, A. S., Laurence, J. A., and Kohut, R. J.: A comparison of indices that describe the relationship between exposure to ozone and reduction in the yield of agricultural crops, Atmospheric Environment (1967), 22, 1229 – 1240, https://doi.org/https://doi.org/10.1016/0004-6981(88)90353-8, 1988.

Li, G., Zhang, R., Fan, J., and Tie, X.: Impacts of black carbon aerosol on photolysis and ozone, Journal of Geophysical Research: Atmospheres, 110, https://doi.org/10.1029/2005JD005898, 2005.

25   Li, G., Bei, N., Cao, J., Wu, J., Long, X., Feng, T., Dai, W., Liu, S., Zhang, Q., and Tie, X.: Widespread and persistent ozone pollution in eastern China during the non-winter season of 2015: observations and source attributions, Atmospheric Chemistry and Physics, 17, 2759–2774, https://doi.org/10.5194/acp-17-2759-2017, https://www.atmos-chem-phys.net/17/2759/2017/, 2017.

Li, Y., Zhang, J., Sailor, D. J., and Ban-Weiss, G. A.: Effects of urbanization on regional meteorology and air quality in Southern California, Atmospheric Chemistry and Physics, 19, 4439–4457, https://doi.org/10.5194/acp-19-4439-2019, https://www.atmos-chem-phys.net/19/4439/2019/, 2019.

Mar, K., Ojha, N., Pozzer, A., and Butler, T.: Ozone air quality simulations with WRF-Chem (v3.5.1) over Europe: Model evaluation and chemical mechanism comparison, Geosci. Model Dev., 9, 3699–3728, https://doi.org/10.5194/gmd-9-3699-2016, 2016.

Mertens, M., Grewe, V., Rieger, V. S., and Jöckel, P.: Revisiting the contribution of land transport and shipping emissions to tropospheric ozone, Atmospheric Chemistry and Physics, 18, 5567–5588, https://doi.org/10.5194/acp-18-5567-2018, https://www.atmos-chem-phys.net/18/5567/2018/, 2018.

Mills, G., Pleijel, H., Malley, C., Sinha, B., Cooper, O., Schultz, M., Neufeld, H., Simpson, D., Sharps, K., Feng, Z., Gerosa, G., Harmens, H., Kobayashi, K., Saxena, P., Paoletti, E., Sinha, V., and Xu, X.: Tropospheric ozone assessment report: Present-day tropospheric ozone distribution and trends relevant to vegetation, Elementa, 6, https://doi.org/10.1525/elementa.302, 2018.

Monks, P. S., Archibald, A. T., Colette, A., Cooper, O., Coyle, M., Derwent, R., Fowler, D., Granier, C., Law, K. S., Mills, G. E., Stevenson, D. S., Tarasova, O., Thouret, V., von Schneidemesser, E., Sommariva, R., Wild, O., and Williams, M. L.: Tropospheric ozone and its precursors from the urban to the global scale from air quality to short-lived climate forcer, Atmospheric Chemistry and Physics, 15, 8889–8973, https://doi.org/10.5194/acp-15-8889-2015, https://www.atmos-chem-phys.net/15/8889/2015/, 2015.

5   Morrison, H., Thompson, G., and Tatarskii, V.: Impact of cloud microphysics on the development of trailing stratiform precip- itation in a simulated squall line: Comparison of one- and two-moment schemes, Monthly Weather Review, 137, 991–1007, https://doi.org/10.1175/2008MWR2556.1, 2009.

Musselman, R., Lefohn, A., Massman, W., and Heath, R.: A critical review and analysis of the use of exposure- and flux-based ozone indices for predicting vegetation effects, Atmospheric Environment, 40, 1869–1888, https://doi.org/10.1016/j.atmosenv.2005.10.064, 2006.

10   Neu, J. L. and Prather, M. J.: Toward a more physical representation of precipitation scavenging in global chemistry models: cloud overlap and ice physics and their impact on tropospheric ozone, Atmospheric Chemistry and Physics, 12, 3289–3310, https://doi.org/10.5194/acp-12-3289-2012, https://www.atmos-chem-phys.net/12/3289/2012/, 2012.

Otero, N., Sillmann, J., Mar, K. A., Rust, H. W., Solberg, S., Andersson, C., Engardt, M., Bergström, R., Bessagnet, B., Colette, A., Couvidat, F., Cuvelier, C., Tsyro, S., Fagerli, H., Schaap, M., Manders, A., Mircea, M., Briganti, G., Cappelletti, A., Adani, M., D'Isidoro, M., 15   Pay, M.-T., Theobald, M., Vivanco, M. G., Wind, P., Ojha, N., Raffort, V., and Butler, T.: A multi-model comparison of meteorological drivers of surface ozone over Europe, Atmospheric Chemistry and Physics, 18, 12 269–12 288, https://doi.org/10.5194/acp-18-12269-2018, https://www.atmos-chem-phys.net/18/12269/2018/, 2018.

Paoletti, E., De Marco, A., and Racalbuto, S.: Why should we calculate complex indices of ozone exposure? Results from Mediterranean background stations, Environmental Monitoring and Assessment, 128, 19–30, https://doi.org/10.1007/s10661-006-9412-5., 2007.

20   Paoletti, E., De Marco, A., Beddows, D., Harrison, R., and Manning, W.: Ozone levels in European and USA cities are increasing more than at rural sites, while peak values are decreasing, Environmental Pollution, 192, 295–299, https://doi.org/10.1016/j.envpol.2014.04.040, 2014.

Pfister, G. G., Avise, J., Wiedinmyer, C., Edwards, D. P., Emmons, L. K., Diskin, G. D., Podolske, J., and Wisthaler, A.: CO source contri- bution analysis for California during ARCTAS-CARB, Atmospheric Chemistry and Physics, 11, 7515–7532, https://doi.org/10.5194/acp-25   11-7515-2011, https://www.atmos-chem-phys.net/11/7515/2011/, 2011.

Pfister, G. G., Walters, S., Emmons, L. K., Edwards, D. P., and Avise, J.: Quantifying the contribution of inflow on surface ozone over Cali- fornia during summer 2008, Journal of Geophysical Research: Atmospheres, 118, 12,282–12,299, https://doi.org/10.1002/2013JD020336, 2013.

Querol, X., Alastuey, A., Gangoiti, G., Perez, N., Lee, H. K., Eun, H. R., Park, Y., Mantilla, E., Escudero, M., Titos, G., Alonso, 30   L., Temime-Roussel, B., Marchand, N., Moreta, J. R., Revuelta, M. A., Salvador, P., Artíñano, B., García dos Santos, S., Anguas, M., Notario, A., Saiz-Lopez, A., Harrison, R. M., Millán, M., and Ahn, K.-H.: Phenomenology of summer ozone episodes over the Madrid Metropolitan Area, central Spain, Atmospheric Chemistry and Physics, 18, 6511–6533, https://doi.org/10.5194/acp-18-6511-2018, https://www.atmos-chem-phys.net/18/6511/2018/, 2018.

Ramaswamy, V., Boucher, O., Haigh, J., Hauglustaine, D., Haywood, J., Myhre, G., Nakajima, T., Shi, G., and 2001, S. S.: Radiative forcing 35   of climate change, In: Climate Change 2001: The Scientific Basis,Contribution of WG1 to the Third Assessment Report of the IPCC, Houghton, J.T. et al. (eds), Cambridge University Press, England, 2001.

Safieddine, S., Boynard, A., Coheur, P.-F., Hurtmans, D., Pfister, G., Quennehen, B., Thomas, J. L., Raut, J.-C., Law, K. S., Klimont, Z., Hadji-Lazaro, J., George, M., and Clerbaux, C.: Summertime tropospheric ozone assessment over the Mediterranean region us-

ing the thermal infrared IASI/MetOp sounder and the WRF-Chem model, Atmospheric Chemistry and Physics, 14, 10 119–10 131, https://doi.org/10.5194/acp-14-10119-2014, https://www.atmos-chem-phys.net/14/10119/2014/, 2014.

Sandu, A. and Sander, R.: Technical note: Simulating chemical systems in Fortran90 and Matlab with the Kinetic PreProcessor KPP-2.1, Atmospheric Chemistry and Physics, 6, 187–195, https://doi.org/10.5194/acp-6-187-2006, https://www.atmos-chem-phys.net/6/187/2006/, 2006.

Stevenson, D. S., Young, P. J., Naik, V., Lamarque, J.-F., Shindell, D. T., Voulgarakis, A., Skeie, R. B., Dalsoren, S. B., Myhre, G., Berntsen, T. K., Folberth, G. A., Rumbold, S. T., Collins, W. J., MacKenzie, I. A., Doherty, R. M., Zeng, G., van Noije, T. P. C., Strunk, A., Bergmann, D., Cameron-Smith, P., Plummer, D. A., Strode, S. A., Horowitz, L., Lee, Y. H., Szopa, S., Sudo, K., Nagashima, T., Josse, B., Cionni, I., Righi, M., Eyring, V., Conley, A., Bowman, K. W., Wild, O., and Archibald, A.: Tropospheric ozone changes, radiative forcing and attribution to emissions in the Atmospheric Chemistry and Climate Model Intercomparison Project (ACCMIP), Atmospheric Chemistry and Physics, 13, 3063–3085, https://doi.org/10.5194/acp-13-3063-2013, https://www.atmos-chem-phys.net/13/3063/2013/, 2013.

Struzewska, J., Zdunek, M., Kaminski, J. W., Łobocki, L., Porebska, M., Jefimow, M., and Gawuc, L.: Evaluation of the GEM-AQ model in the context of the AQMEII Phase 1 project, Atmospheric Chemistry and Physics, 15, 3971–3990, https://doi.org/10.5194/acp-15-3971-2015, https://www.atmos-chem-phys.net/15/3971/2015/, 2015.

Sudo, K. and Akimoto, H.: Global source attribution of tropospheric ozone: Long-range transport from various source regions, Journal of Geophysical Research Atmospheres, 112, https://doi.org/10.1029/2006JD007992, 2007.

Tagaris, E., Stergiou, I., and Sotiropoulou, R.: Impact of shipping emissions on ozone levels over Europe: assessing the relative importance of the Standard Nomenclature for Air Pollution (SNAP) categories, Environmental Science and Pollution Research, 24, 14 903–14 909, https://doi.org/0.1007/s11356-017-9046-x, https://doi.org/10.1007/s11356-017-9046-x, 2017.

Tai, A. P. and Val Martin, M.: Impacts of ozone air pollution and temperature extremes on crop yields: Spatial variability, adaptation and implications for future food security, Atmospheric Environment, 169, 11 – 21, https://doi.org/https://doi.org/10.1016/j.atmosenv.2017.09.002, 2017.

Tang, Y., Carmichael, G., Thongboonchoo, N., Chai, T., Horowitz, L., Pierce, R., Al-Saadi, J., Pfister, G., Vukovich, J., Avery, M., Sachse, G., Ryerson, T., Holloway, J., Atlas, E., Flocke, F., Weber, R., Huey, L., Dibb, J., Streets, D., and Brune, W.: Influence of lateral and top boundary conditions on regional air quality prediction: A multiscale study coupling regional and global chemical transport models, Journal of Geophysical Research Atmospheres, 112, https://doi.org/10.1029/2006JD007515, 2007.

Thouret, V., Cammas, J.-P., Sauvage, B., Athier, G., Zbinden, R., Nédélec, P., Simon, P., and Karcher, F.: Tropopause referenced ozone climatology and inter-annual variability (1994–2003) from the MOZAIC programme, Atmospheric Chemistry and Physics, 6, 1033–1051, https://doi.org/10.5194/acp-6-1033-2006, https://www.atmos-chem-phys.net/6/1033/2006/, 2006.

Tie, X., Madronich, S., Walters, S., Zhang, R., Rasch, P., and Collins, W.: Effect of clouds on photolysis and oxidants in the troposphere, Journal of Geophysical Research: Atmospheres, 108, https://doi.org/10.1029/2003JD003659, 2003.

Tong, D., Mathur, R., Kang, D., Yu, S., Schere, K., and Pouliot, G.: Vegetation exposure to ozone over the continental United States: Assessment of exposure indices by the Eta-CMAQ air quality forecast model, Atmospheric Environment, 43, 724–733, https://doi.org/10.1016/j.atmosenv.2008.09.084, 2009.

Tuccella, P., Curci, G., Visconti, G., Bessagnet, B., Menut, L., and Park, R.: Modeling of gas and aerosol with WRF/Chem over Europe: Evaluation and sensitivity study, Journal of Geophysical Research Atmospheres, 117, https://doi.org/10.1029/2011JD016302, 2012.

UNECE: Mapping Critical Levels for Vegetation. International Cooperative Programme on Effects of Air Pollution on Natural Vegetation and Crops, Bangor, UK, 2010.

Vijayaraghavan, K., Cho, S., Morris, R., Spink, D., Jung, J., Pauls, R., and Duffett, K.: Photochemical model evaluation of the ground-level ozone impacts on ambient air quality and vegetation health in the Alberta oil sands region: Using present and future emission scenarios, Atmospheric Environment, 141, 209–218, https://doi.org/10.1016/j.atmosenv.2016.06.053, 2016.

Wang, Z., Chien, C.-J., and Tonnesen, G.: Development of a tagged species source apportionment algorithm to characterize three-dimensional transport and transformation of precursors and secondary pollutants, Journal of Geophysical Research Atmospheres, 114, https://doi.org/10.1029/2008JDO10846, 2009.

Wesely, M.: Parameterization of surface resistances to gaseous dry deposition in regional-scale numerical models, Atmospheric Environment (1967), 23, 1293–1304, https://doi.org/10.1016/0004-6981(89)90153-4, 1989.

Westenbarger, D. A. and Frisvold, G.: Air pollution and farm level crop yields: an empirical analysis of corn and soybeans, Agric. Resour. Econ. Rev., 24 (1995), 156–165, 1995.

WHO: Quantification of health effects of exposure to air pollution, EUR/01/5026342, E74256, WHO Regional office for Europe, Copenhagen, Available at: http://www.euro.who.int/document/e74256.pdf (last accessed 20 April 2018), 2001.

WHO: Air quality guidelines. Global update 2005. Particulate matter, ozone, nitrogen dioxide and sulfur dioxide, World Health Organizations 2006, pp. ix+484 pages, ISBN 9289021 926, https://doi.org/http://www.euro.who.int/__data/assets/pdf_file/0005/78638/E90038.pdf?ua=1 (last accessed, 18 April 2016), 2006.

WHO: Evolution of WHO air quality guidelines: past, present and future, World Health Organizations, (last accessed 1 August 2017), pp. vi+32 pages, https://doi.org/ISBN9789289052306, 2017.

Wiedinmyer, C., Akagi, S. K., Yokelson, R. J., Emmons, L. K., Al-Saadi, J. A., Orlando, J. J., and Soja, A. J.: The Fire INventory from NCAR (FINN): a high resolution global model to estimate the emissions from open burning, Geoscientific Model Development, 4, 625–641, https://doi.org/10.5194/gmd-4-625-2011, https://www.geosci-model-dev.net/4/625/2011/, 2011.

Yarwood, G., Morris, R., Yocke, M., Hogo, H., and Chico, T.: Development of a Methodology for Source Apportionment of Ozone Concentrations Estimates From a Photo-chemical Grid Model, Air and Waste management association, p. 15222, 1996.

Table 1. List of tagged source regions and global source types

Category	Acronym	List of countries or global source types
European source regions	MBS	Mediterranean, and Black Seas
	BNS	Baltic, and North Seas
	CEE	Central-East Europe includes East Austria, Hungary, Czech Republic, Slovakia, Estonia, Latvia, Lithuania, Poland
	ALP	High Alps (West Austria, Switzerland, and North Italy) and Po Valley
	ITA	South Italy, and Malta
	SEE	South-East Europe includes Bulgaria, Romania, Moldavia, Albania, Slovenia, Croatia, Serbia, Montenegro, Macedonia, Greece, and Cyprus
	IBE	Iberia includes Spain, and Portugal
	UKI	United Kingdom, and Ireland
	GEN	Germany, Belgium, Netherlands, and Luxembourg
	SCA	Scandinavia (Finland, Norway, Sweden), Denmark, and Island
	FRA	France
	RBU	Russia, Belarus, and Ukraine
	TCA	Turkey, Azerbaijan, Armenia, and Georgia
HTAP2 source regions	ASI	Chemical boundary condition of modelled species coming from Asia
	NAF	Chemical boundary condition of modelled species coming from North-Africa
	NAM	Chemical boundary condition of modelled species coming from North-America
	OCN	Chemical boundary condition of modelled species coming from shipping activities
	RST	Chemical boundary condition of modelled species coming from rest of the world
Global source types	BIO	biogenic
	BMB	biomass burning
	LGT	lightning
	STR	stratospheric O3

Table 2. Observed mean and simulation summary statistics for meteorological parameters. The normalized mean bias (NMB) and correlation coefficient (R) are calculated between simulated and observed meteorological observation from GWO during April – September 2010 period

Variable	Observed			Modelled mean			NMB (%)	R
	min	mean	max	min	mean	max		
MSLP (hPa)	1000.96	1014.3	1022.06	969.05	1014.5	1039.03	-0	0.98
T2M (°C)	-17.14	14.99	32.10	-22.50	14.76	43.45	-3	0.91
WS10M (m/s)	0.36	3.37	10.83	0.00	3.59	20.41	8	0.65
WD10M (°)	0	190	360	31.91	216	318	13	0.47

Table 3. Observed mean and simulation summary statistics for MDA8 O_3 concentrations ($\mu g/m^{-3}$) at rural background sites. The normalized mean bias (NMB) and correlation coefficient (R) are calculated between simulated and observed O_3 concentrations from the AirBase dataset during April – September 2010 period.

Analyzed period	Observed			Modelled			NMB (%)	R
	min	mean	max	min	mean	max		
April	52.5	97.0	140.8	36.5	90.8	134.5	-6.3	0.58
May	41.0	87.9	143.0	28.0	83.2	124.6	-5.4	0.62
June	44.2	96.2	162.3	32.0	89.7	132.6	-6.8	0.71
July	43.8	97.0	178.2	26.0	90.8	147.7	-6.3	0.58
August	40.3	87.5	145.2	27.3	82.6	130.8	-5.6	0.65
September	33.4	77.5	135.4	26.5	81.1	129.6	4.6	0.63
Total	40.5	90.5	160.5	28.4	86.3	135.9	-5.2	0.69
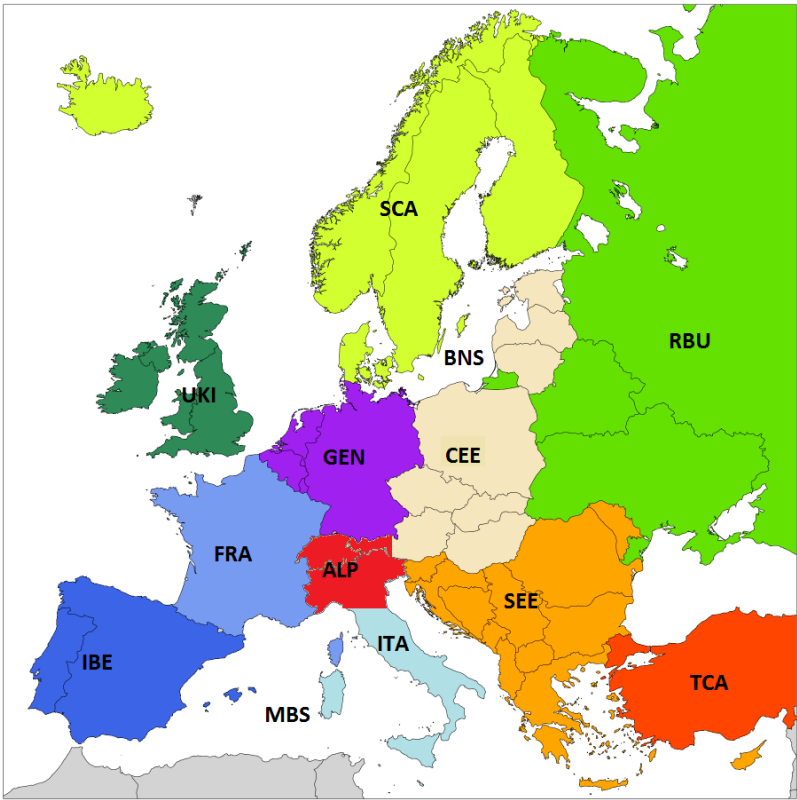
Figure 1. Tagged European source regions

MDA8 O3 (ppb) - April-May 2010
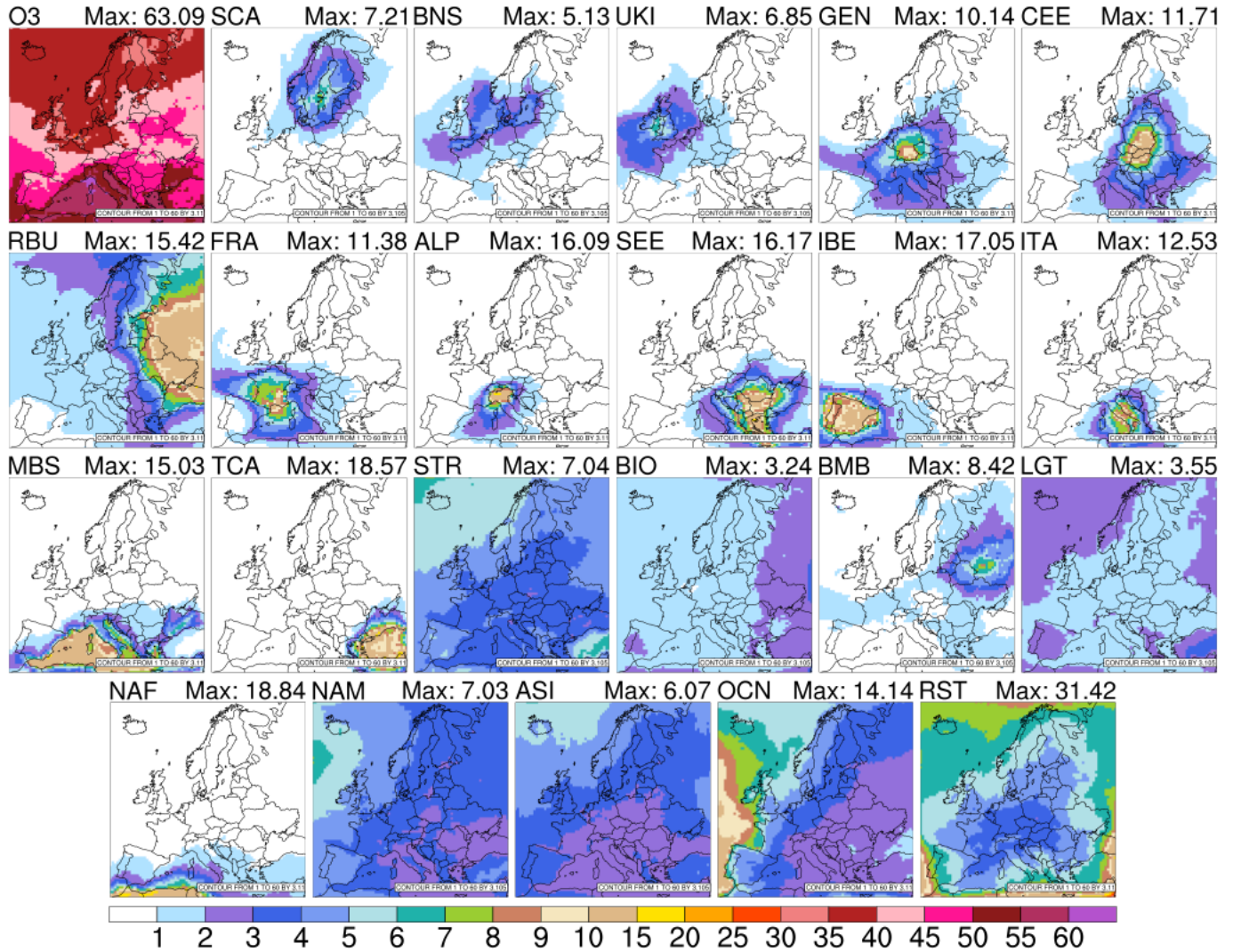
Figure 2. Contribution to MDA8 O$_3$ (ppb) of each O$_3$ source region and global source type for the April-May 2010 period

MDA8 O3 (ppb) - June-August 2010
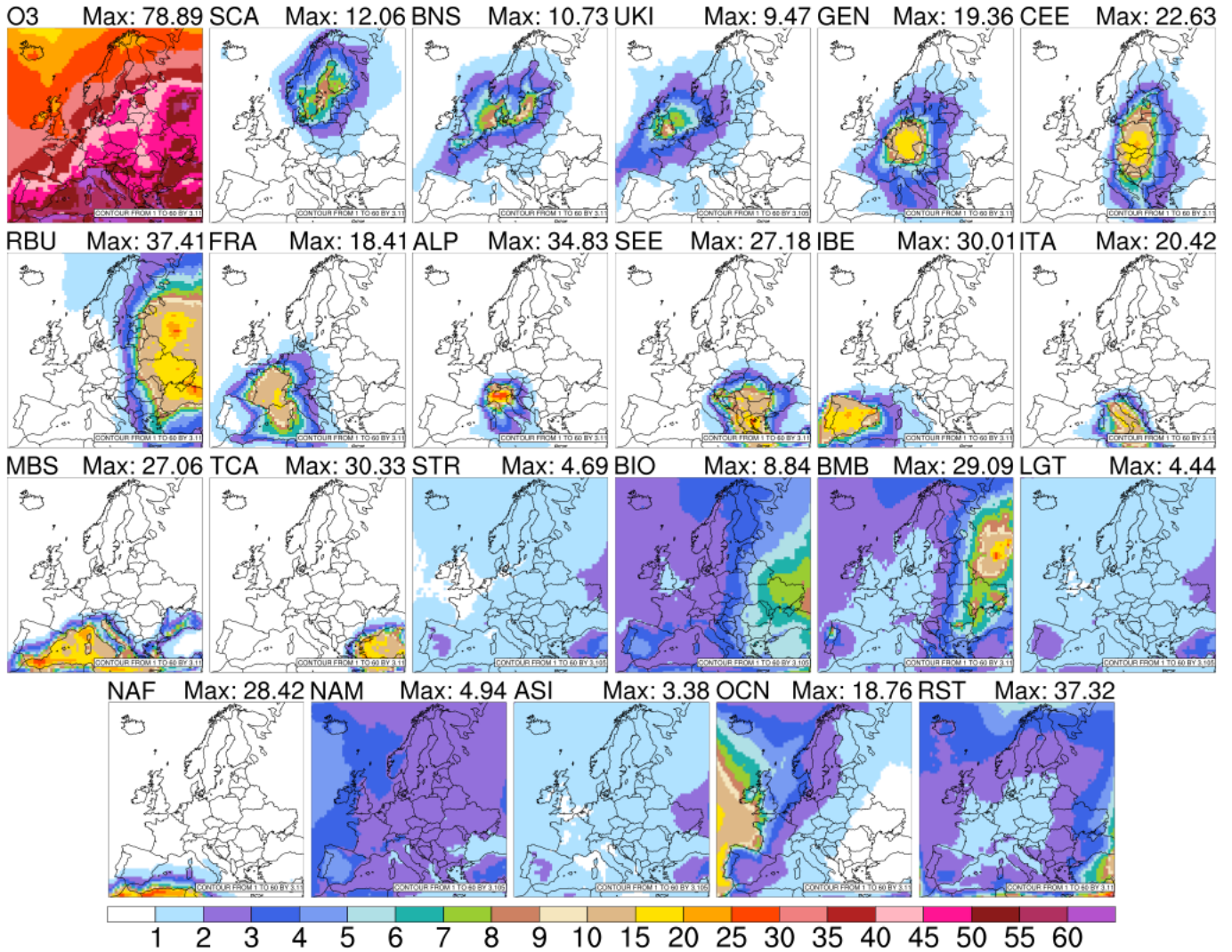
Figure 3. Same as Fig. 2, but for the June-August 2010 period
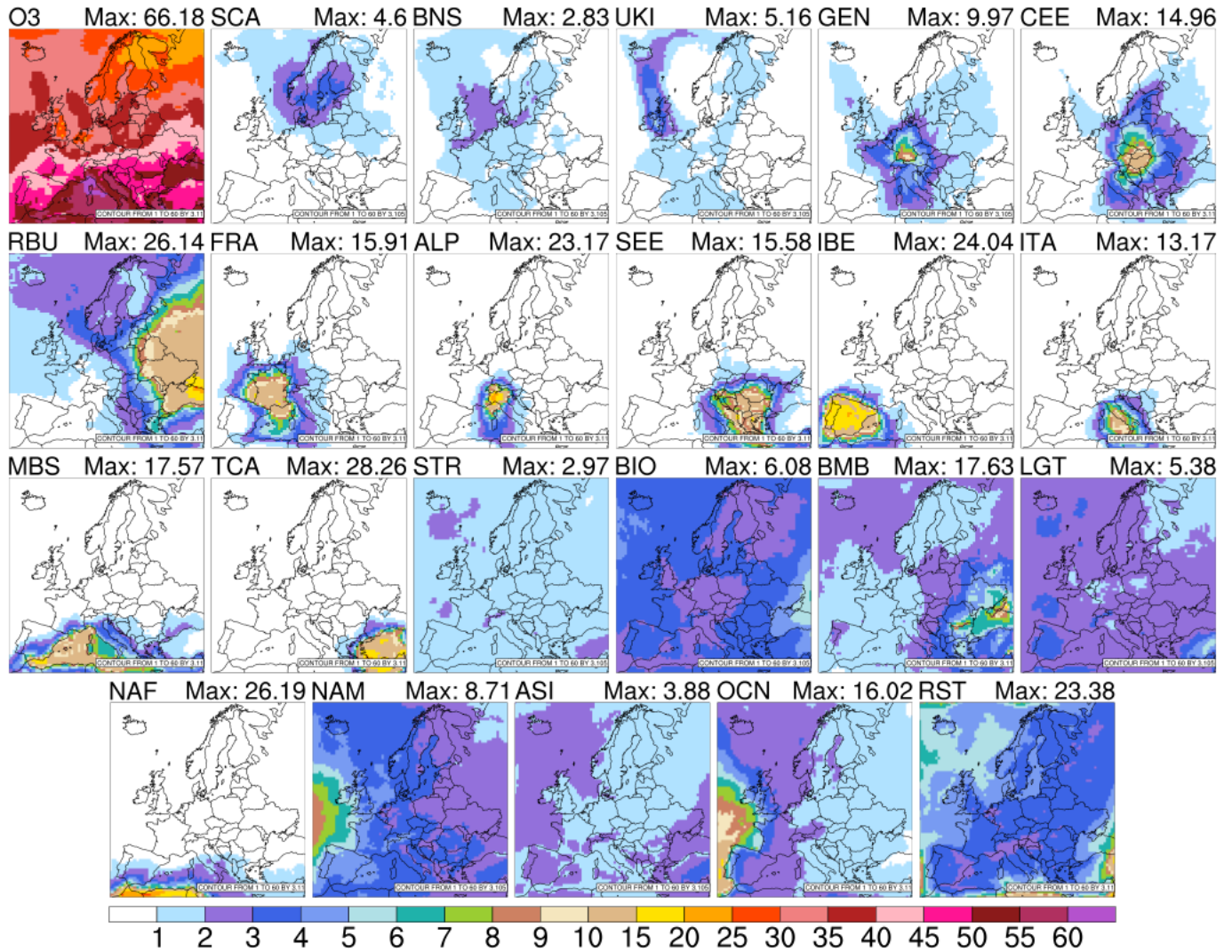
Figure 4. Same as Fig. 2, but for September 2010
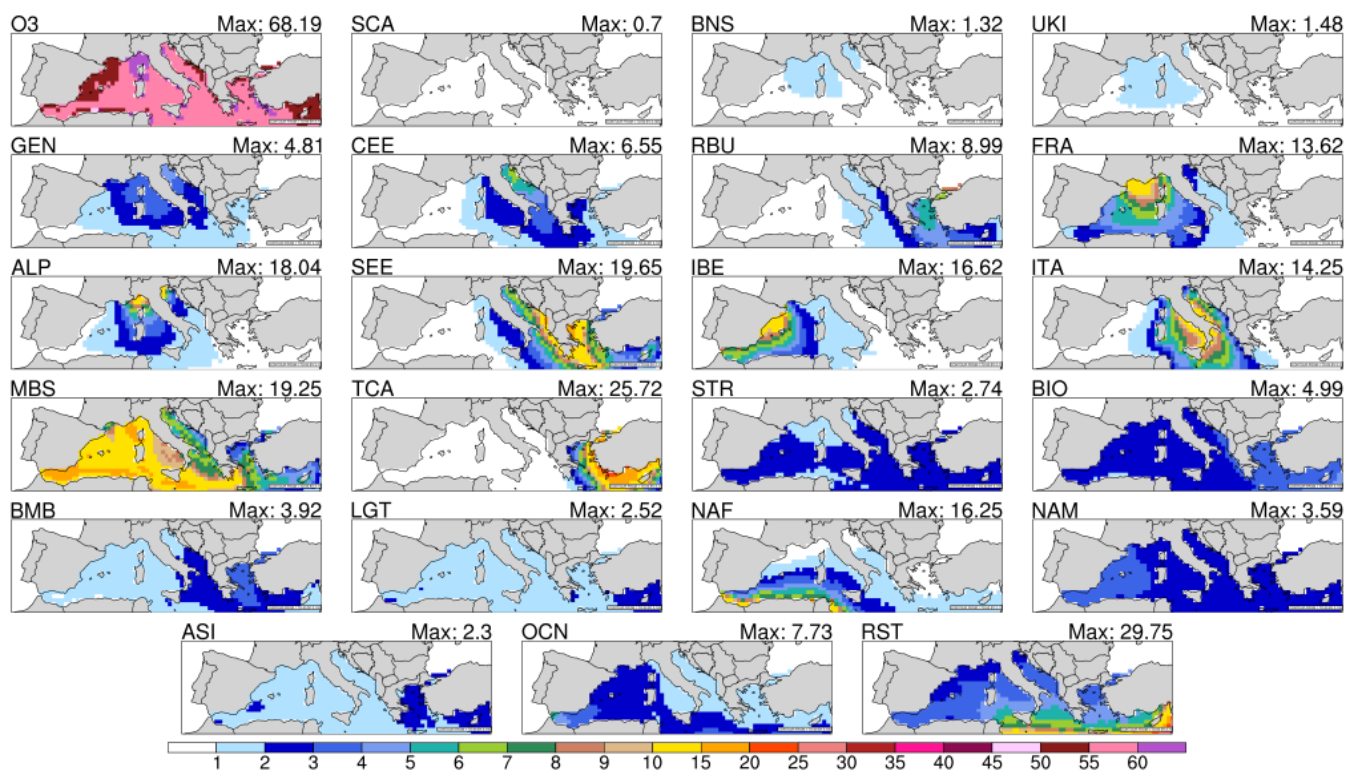
Figure 5. Average MDA8 O₃ mixing ratio (upper left panel) and contribution of each tagged O₃ source region and global source type over the Mediterranean Sea for the April-September 2010 period. The unit is ppb
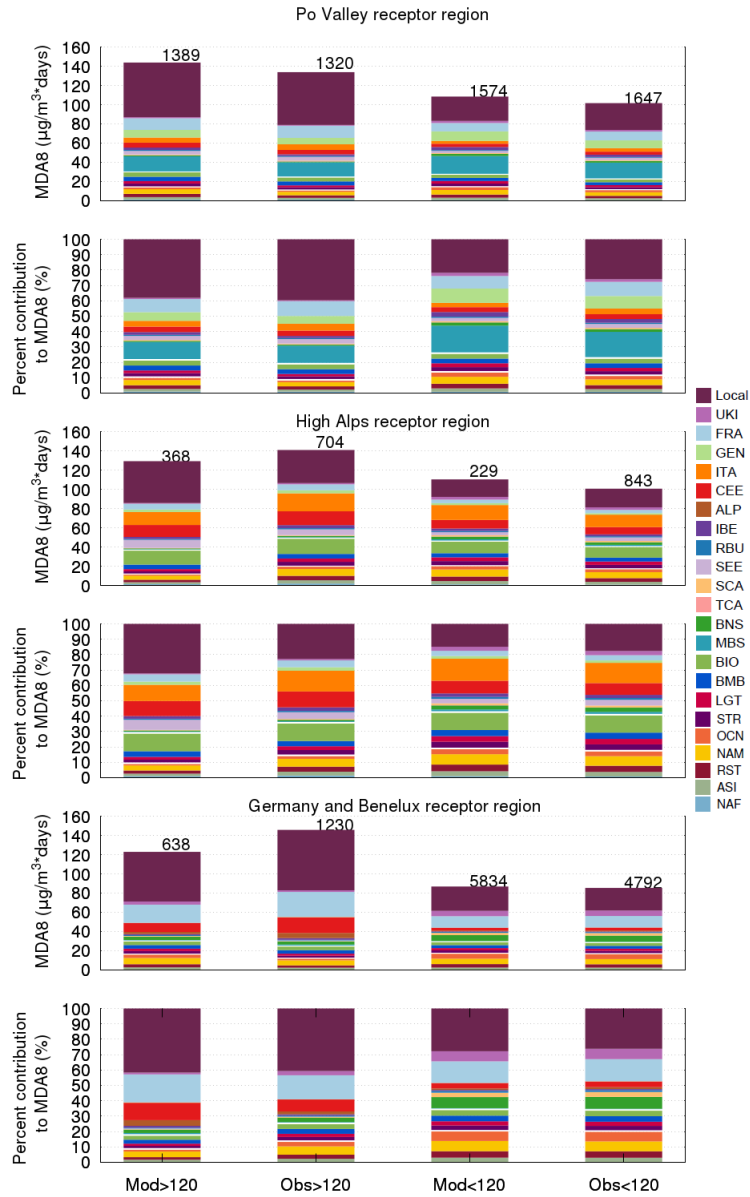
Figure 6. Mean modelled and observed MDA8 O₃ mixing ratio filtered by a threshold of 120 μ g m^{-3} for Po Valley, (top panel) high Alps (third from top panel) and GEN (fifth from top panel) and percent contribution to MDA8 O₃ from different emissions sources and types for Po Valley (second panel), high Alps (fourth) and GEN (bottom panel) during April-September 2010 period. In each case the contributions of tagged sources to the total O₃ are shown. The tagged contributions of local and other European sources, HTAP2 source regions and other global source types to observed O₃ are obtained by scaling the observed O₃ by the relative contributions of these tagged sources to modelled O₃. The total number of exceedances (and non-exceedances) of the MDA8 O₃ target value is indicated at the top of each column

Figure 7. Comparison of percent contribution of local and other European sources, HTAP2 source regions and other global source types to different to O₃ metric. The metrics analysed are mean, MDA8 and 95th percentile (ppb) for the early "F" and late "S" simulation period, W126 (ppm − hours), SOMO35 and AOT40 (ppb − hours). The white dashed lines on each panel separate different categories (intercontinental transport, other global source types, and local and other European sources)
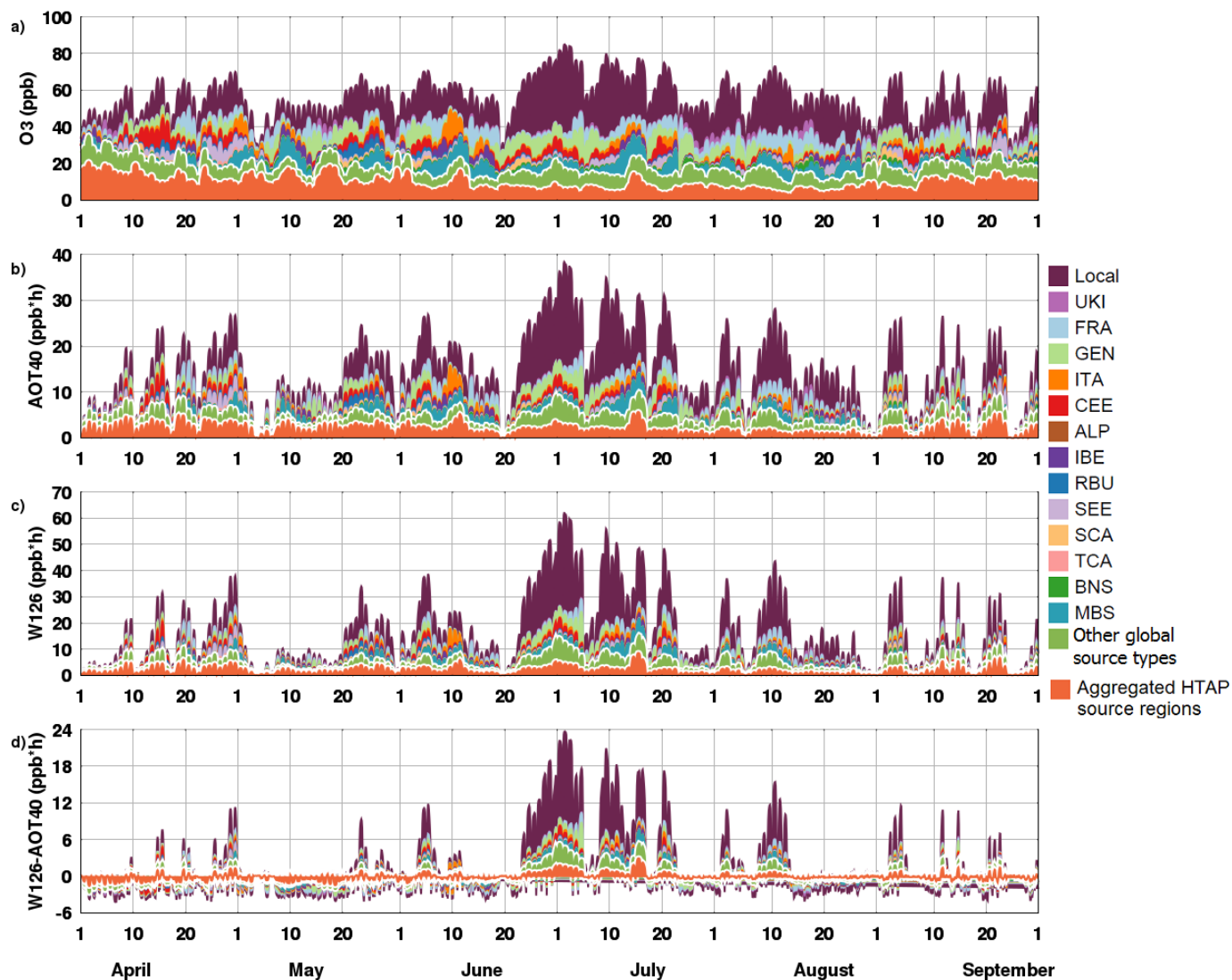
Figure 8. April-September 2010 time series of daytime a) hourly O_3 (ppb), b) hourly AOT40 index (ppb − hours), c) hourly W126 index (ppb − hours) and d) differences between W126 and AOT40 indexes (ppb − hours) averaged over Po Valley receptor region. The colour bars indicate the O_3 source categories - aggregated HTAP2 regions (ASI, NAM, NAF, OCN and RST), the other global source types (STR, LGT, BMB and BIO) and the European source regions. The white dashed lines on each panel separate different categories (intercontinental transport, other global source types, and local and other European sources).
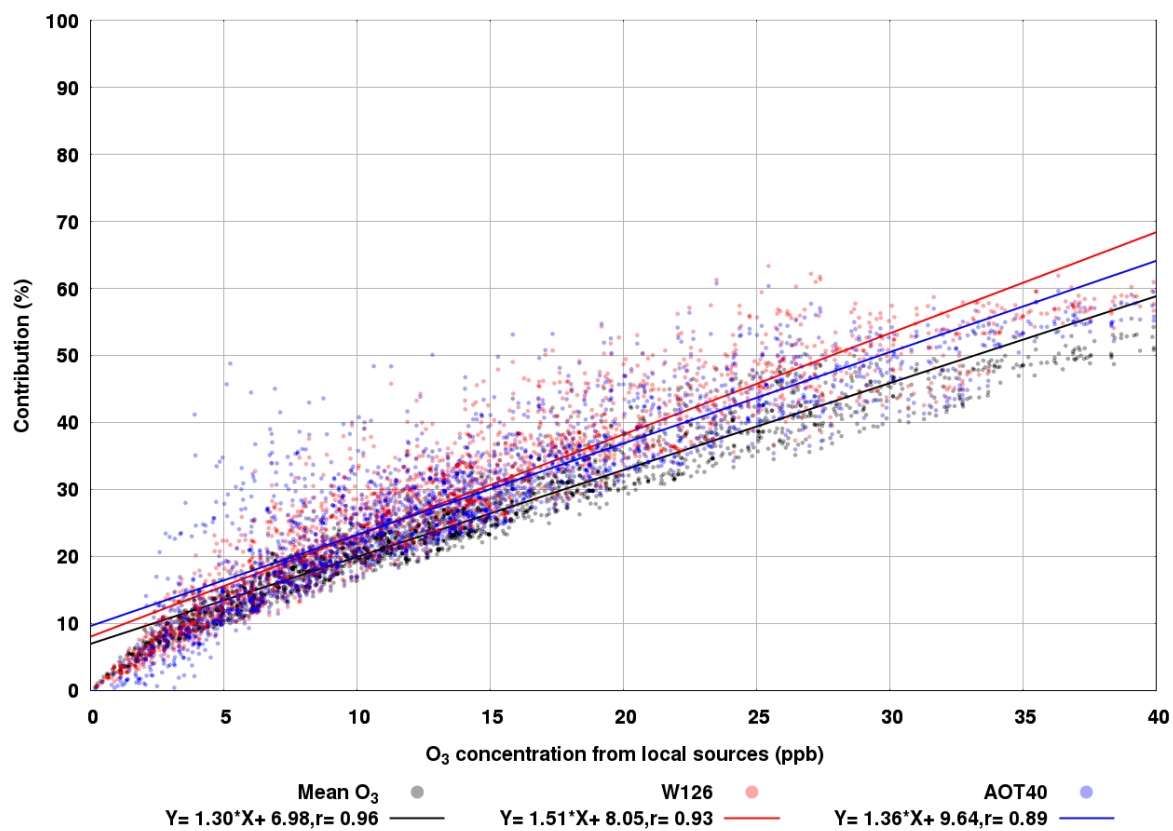
Figure 9. Scatter plots showing the ozone concentration from local sources versus the contribution to Mean O_3 (black dots), W126 (red dots) and AOT40 (blue dots). The solid lines are the lines of best fit.